SPECTRUM LOADING AND MULTIDIRECTIONAL SLIDING OF PTFE WITH A PIN-ON-FLAT TRIBOMETER

By

DARREN MCGUIRE

A THESIS PRESENTED TO THE GRADUATE SCHOOL
OF THE UNIVERSITY OF FLORIDA IN PARTIAL FULFILLMENT
OF THE REQUIREMENTS FOR THE DEGREE OF
MASTER OF SCIENCE

UNIVERSITY OF FLORIDA

2003

ACKNOWLEDGMENTS

I would like to acknowledge all those that helped make the culmination of my academic career a reality. I cannot express the debt of gratitude I feel nor stress the importance of every person's contribution to my thesis project. However, I would at least like to point out a few that made it possible.

I thank Howard Purdy for his machining efforts, Gregory Sawyer for his guidance, knowledge, and friendship, Dr. Ziegert , Dr. Arakere, and Dr. Schueller for their review of this thesis and assistance in the classroom and lab throughout the course of my entire education, and members of the tribology lab for their suggestions, perspectives, and support.

Most of all I would like to thank my parents and family. Emotions can leave words far in the distance and I find none that can explain what they mean to me. I love them more than life itself.

TABLE OF CONTENTS

Page

LIST OF TABLES

LIST OF FIGURES

Abstract of Thesis Presented to the Graduate School
of the University of Florida in Partial Fulfillment of the
Requirements for the Degree of Master of Science

SPECTRUM LOADING AND MULTIDIRECTIONAL SLIDING OF PTFE WITH A PIN-ON-FLAT TRIBOMETER

By

DARREN MCGUIRE

August 2003

Chair: W. Gregory Sawyer
Cochair: John Ziegert
Major Department: Mechanical and Aerospace Engineering

Wear is a process of gradual breakdown or removal of material by relative motion between two contacting surfaces. In this report, the wear of polytetrafluoroethylene (PTFE) under spectrum loading and multidirectional sliding was investigated. Wear tests revealed a strong proportional dependence on load but showed no dependence on sinusoidal fluctuations in load. Abrupt changes in the direction of motion, known as reversal zones, correlated with increases in wear, meaning the more reversal zones present on a motion path, the more severe the wear was compared to a motion path with no reversal zones (circular). Multidirectional sliding appeared to have no influence on overall wear. This differs greatly with what is known about the wear behavior of ultra high molecular weight polyethylene (UHMWPE). The difference may stem from a delamination process that takes place during PTFE sliding. Using data collected from a

white light interferometer, a model of the counterface surface was constructed, and when applied to the polymer pin using Hertzian contact assumptions induced a pressure profile that yields subsurface shear stresses. The magnitude of the subsurface shear stresses shows no dependence on direction of sliding. This is offered as an explanation for the lack of increased wear during multidirectional sliding over unidirectional sliding. Finally a correlation between number of cycles incurred over a wear path and wear rate is observed. A simple model using rules of linear mixing was constructed for wear predictions based on single point mass loss measurements.

CHAPTER 1
INTRODUCTION

Wear is defined by the dictionary as "to impair, deteriorate, or consume gradually by use or any continued process." From an engineering standpoint, wear maybe be described as the gradual breakdown or removal of material stemming from relative motion between two contacting surfaces. Wear of special polymers such as polytetrafluoroethylene (PTFE) and ultra high molecular weight polyethylene (UHMWPE) has become a major concern due to their effectiveness as biocompatible materials. Despite the success of polymers as bearing surface for total knee or hip replacements in treatment of end stage arthritis, the gradual breakdown of these surfaces has led to component loosening and an eventual need for revision surgery.

The mechanisms that cause removal of material can be resolved into abrasive, adhesive, and fatigue wear. Abrasive wear occurs when asperity peaks on the harder surface scratch away material on the softer surface. Adhesive wear occurs when bonding forces between the two surfaces are strong enough to pull material away from one or both surfaces as relative motion occurs between them. Fatigue wear occurs when material is removed as a result of cyclic stresses that exceed the fatigue strength of the material [50]. Each mechanism's contribution to wear is difficult to observe when all three factors are acting simultaneously. Minimizing the wear mechanisms that are not of interest allows the remaining mechanisms to dominate the wear process. Therefore, an observation of a

single desired mechanism or a combination of desired mechanisms affects could be made.

Throughout this paper adhesive wear will always be a central focus. Several wear tests will be run with the interest of investigating behavior of adhesive wear as well as behavior of adhesive and fatigue wear in combination. The tests presented in this paper all involve PTFE in contact with stainless steel counterfaces. For the case in which one of the two surfaces in contact is significantly harder than the other surface, minimizing abrasive wear requires that the harder surface be highly polished, thereby limiting the material scratched away from the softer surface to an insignificant amount. Under dry testing, wear rates for PTFE and UHMWPE are known to increase dramatically when in contact with counter faces displaying and average roughness (Ra) greater than 0.1μm. Fatigue wear can be virtually eliminated by maintaining the load holding the two surfaces in contact constant. However, some cyclical effects will be present as the frictional force vector changes direction along with changes in the sliding path direction.

Wear rate is a key factor in characterizing a materials performance in wear testing. If wear rate is known prior to testing, predictions about how much material will be lost during the course of a test can be made. However, wear rate does not always remain constant and may change depending on the testing parameters implemented. Although the molecular structures for both PTFE and UHMWPE are similar, their wear behavior differs drastically. UHMWPE wear is dominated by a surface phenomenon that is highly dependent on changes in the direction of sliding. However, PTFE shows no directional dependence and appears to wear from a subsurface phenomenon known as delamination. A process where subsurface imperfections or cracks are forced to propagate due to

subsurface stresses incurred during sliding. The cracks propagate and link up with one another forming larger cracks. These cracks continue to propagate and eventually turn towards the surface breaking off a flake of wear debris. This process repeats through out the duration of sliding. However, the wear process has been shown to depend on the development of a transfer film. This indicates that the wear process is not completely driven by the bulk material, but depends on the surface interactions between bulk and counterface.

CHAPTER 2
REVIEW OF LITERATURE

2.1 Proposed Mechanisms of Wear for PTFE

With all the recent interest surrounding UHMWPE and its use in human joint replacements many experiments have been compiled in hopes of developing a predictive wear model. Sliding wear of UHMWPE is described as a surface wear phenomenon where the molecular chains align themselves with the direction of sliding. Once the molecular chains align themselves with the direction of sliding, wear rate drops significantly. If the direction of sliding changes, wear rate increases until the chains can reorient themselves and wear rate drops once again. If the direction of sliding is always changing there is no preferred molecular orientation and wear rate remains significantly higher than under unidirectional sliding. Although PTFE and UHMWPE have similar molecular composition their wear behaviors differ drastically in that PTFE is considered to have poor wear resistance.

Tanaka, Uchiyama, and Toyooka [1] performed early investigations into the wear of PTFE. They observed that when slid against a glass plate, PTFE deposited a fibrous thin film with long bands and striations perpendicular to the length of the bands. At a sliding speed of 20 cm/s, the PTFE wear was shown to increase linearly with increasing sliding distance while the friction measured during sliding initially decreased before settling to a constant value. The initial drop off in friction is attributed to formation of the PTFE transfer film. Tanaka later demonstrated that varying the sliding rate produced

a change in the PTFE wear rate. Sliding a 5 cm/s resulted in an initial high wear rate that quickly transitioned to a slower wear rate. He also showed that at temperatures below 100°C the wear rates would peak for a given sliding speed, and that these peaks shifted to higher speeds as the temperature was increased. Whereas for temperatures above 100°C the peaks tended to shift towards lower speeds as temperature was increased. Friction decreased with increasing temperature and increased with increasing sliding speed. Tanaka also used a thermocouple to measure the temperature rise at the sliding surface, and concluded that the temperature rise due to frictional heating was insignificant. This was attributed to the rapid removal of PTFE during sliding and the transfer film's aid in heat dissipation. Inspection of the worn surfaces revealed that the same wear mechanism of PTFE acted under all circumstances. The molecular orientation and the uniform separations of striations in the transfer films indicate that the PTFE fibers are held together by lateral connections. Tanaka states that the explanation for PTFE's high wear rate stems from the lack of melting at the PTFE/Substrate interface and the easy removal of film from the substrate. Inspection of the transfer film reveals that a thin layer of amorphous PTFE is likely removed from the bulk during sliding. The shearing that occurs during sliding causes slippage in the amorphous region and the PTFE is then deposited in slices. Given this, Tanaka attributes the effect of sliding speed on friction and wear to the likelihood of viscoelastic behavior between these slices. When abrasive wear is present the slippage between slices does not occur and no film is observed. This is due to the severe damage caused by abrasive wear.

In 1977 Tanaka and Miyata [2] published a study of PTFE cylinders slid on glass plates. The study into the friction and transfer of semi-crystalline polymers reveled that

adhesion of the molecular chains in PTFE is stronger when the direction of sliding is perpendicular to the orientation of the molecular chains. This was contradictory to previously understood results. Tanaka and Miyata examined the transfer films after several increments in traverse. They observed that the transfer film thickness increased with increasing traverses. However, they limited the number of traverses to twenty. They were also able to observe that the kinetic friction value remained constant for all traverses. This suggests that shearing occurs within the PTFE transfer film. Tanaka and Miyata also suggest that the banded structure of the PTFE film as well as adsorption of water molecules on the PTFE molecular chains reduces shearing strength on the PTFE surface. However, they go on to suggest that the friction behavior and transfer of PTFE during sliding is mainly influenced by the molecular profile and not by the banded structure. Tanaka previously found that film thickness formation of about 300 angstroms is based on mutual slippage of the crystalline slices in the banded structure, but was unable to apply these findings to the current experiments.

The prevailing model for PTFE transfer from bulk to substrate under reciprocating conditions is that of very long, straight, and crystalline ribbons. Using a oxide-covered Si wafer, M. Schott [3] observed that these ribbons cover nearly the entire substrate and stated that the morphology of the films depends on the temperature at which sliding takes place, the speed at which the PTFE bulk slides relative to the substrate, and the normal load applied to the PTFE bulk while sliding. Schott chose to indicate the loading conditions as weights in order to deduce the nominal pressures. Both the PTFE and substrate were kept at the same temperature and sliding speed was kept low and smooth (0.4 to 2 mm/s). Schott's experiments were conditioned by allowing the starting PTFE

material to be removed before the transfer film was formed. Using IR transmission data, nuclear reaction analysis, and atomic force microscopy Schott was able to confirm the presence of a highly oriented PTFE transfer film.

Bodo and Schott [4] did a second investigation into the formation of highly oriented PTFE films in which a PTFE rod was slid against an oxide-covered silicon wafer under controlled load and temperature. The PTFE samples were "conditioned" by prior sliding to eliminate the initial rapid wear phase of PTFE. Schott again saw the classical characteristics of a PTFE transfer film. However, he was able to generalize the films into three different categories. The first group consisted of irregular ribbons and low coverage (20% of wear path). Both the second and third groups showed long, straight, and parallel ribbons, but the second group had incomplete coverage while the third had complete coverage. Schott reported that the first group appeared during tests run at temperatures under 150°C. The ribbons showed kinks and branching. He also states that although the ribbons consisted of bundles of polymer chains running parallel to the ribbons, the ribbons appeared considerably longer than the macromolecule in the PTFE. Schott goes on to state that the ribbons are formed during or after film deposition. The second type of film occurred during tests run above 150°C and the third occurred above 220°C and 600g loads. However, the coverage decreased to 76% when the load was increased to 2425g. The film cross-sectional thickness increased only slightly with increasing temperature. Schott acknowledges that film variations may result from variations in sample-substrate contact. He suggests that at high temperatures and loads, the variations diminish due to higher plastic deformation. Schott also reports that the film morphology is independent of substrate material and is a property of PTFE only.

Using the concept of dimensional analysis, Kar and Bahadur developed an equation describing the wear of polymers in 1974. The Kar and Bahadur equation was a function of pressure P, speed *v*, time T, modulus of elasticity E, surface energy γ, thermal conductivity K and specific heat C_p. The dimensional analysis yielded an equation for volume loss represented by:

$$V = kP^x v^{y-z} T^y \gamma^{3-y+a} E^{-3-x+y} \left(\frac{C_p}{K} \right)^z \tag{1}$$

where x, y, and z are exponents determined experimentally. In 1995 Viswanath and Bellow [5] extended the Kar and Bahadur equation to include counterface surface roughness. Viswanath and Bellow again used dimensional analysis to derive a dimensionally homogeneous equation that included the specified variables. Viswanath and Bellow included five dimensionless groups comprised of wear volume V, surface energy γ, modulus of elasticity E, specific heat C_p, thermal conductivity K, contact force W, counterface roughness α, sliding speed *v*, and time T. The groups signify dependence on interface contact and deformation (VE^3/γ^3) , normal load and strength characteristics (WE/γ^2), speed and temperature (TEC_p/K), counterface roughness ($\alpha E/\gamma$), and thermal contributions ($\gamma C_p/vK$) yielding the dimensionless function:

$$\Psi\left(\frac{VE^3}{\gamma^3}, \frac{WE}{\gamma^2}, \frac{vK}{\gamma C_p}, \frac{TEC_p}{K}, \frac{\alpha E}{\gamma} \right) = 0 \tag{2}$$

Viswanath and Bellow then applied a non-linear relationship to map their experimental results.

$$V = kW^p v^q T^r \alpha^s E^{-3+p+r+s} \gamma^{3-2p-q-s} \left(\frac{C_p}{K} \right)^{r-q} \tag{3}$$

where p, q, r, and s are exponents determined experimentally. They found, for a pin-on-disk configuration with steel counterfaces, Equation (3) allows a predictive model for volume losses based on operating and material factors know to affect wear.

In 1990, Yang et al. [6] investigated the effect of temperature on the formation of transfer films. Yang and Hirvonen used a pin-on-plate configuration to produce sliding of a PTFE specimen on a stainless steel counterface. They used γ-ray yield curves to verify the amount of PTFE transferred during sliding. They were able to observe that the deposition rate was higher during the first traverse of unidirectional sliding, and that prolonged sliding could be modeling using a linear equation:

$$x = x_0 + \upsilon(n-1) \tag{4}$$

where x is the amount of PTFE transferred, x_0 is the amount transferred after the first traverse, v is the steady-state transfer rate, and n is the number of traverses. They also observed that transfer rate depended on temperature. Their normalized data indicated that thickness increased less rapidly with increasing temperature as the number of traverses was increased. They model this using the following equation:

$$x(T,n) = x(T_{rt},n)g(T) \tag{5}$$

where $x(T,n)$ and $x(T_{rt},n)$ are the thicknesses of the transferred PTFE after n traverses at room temperature and temperature T, and g(T) is a temperature enhancement factor. Despite variations in transfer film appearance at certain temperatures and qualitative disagreement with transfer and PTFE hardness, Yang and Hirvonen concluded that transfer of PTFE during the first traverse increases non-linearly by approximately an order of magnitude when increasing temperature from room to 200°C. However, the

steady-state transfer rate at room temperature and 100°C are virtually the same while transfer at 200°C is increased significantly.

Using a pin-on-disk configuration, Blanchet and Peng [7] published an investigation into irradiated PTFE wear on stainless steel. Irradiating PTFE causes primary and secondary radicals to form by severing the C-C and C-F bonds. The radicals then recombine to form a cross-linked network that has been shown to offer better wear resistance than the original linear PTFE molecular structure. Blanchet and Peng showed that the wear rate of PTFE decreased as irradiation dose increased from 0 to 30 Mrad then increased somewhat as the irradiation dose increased from 30 to 100 Mrad. They also observed that the hardness of PTFE increased from R_h = 43 to 53 over the same 0 to 30 Mrad dose. Friction was also found to increase as the irradiation dose increased from 0 to 5 Mrad. However, friction was then observed to decrease as to dose increased to 20 Mrad then settled to a constant value that was comparable to the coefficient of friction of unirradiated PTFE. In addition to these findings, they also observed a change in the wear debris morphology. Unirradiated PTFE is known to produce large plate like wear debris where as the irradiated PTFE yielded a very fine debris. Blanchet and Peng concluded that the difference in properties between unirradiated and irradiated PTFE was due to the branched and cross-linked network preventing molecular orientation. Molecular orientations of PTFE chains result in low shear strength and the subsequent formation of transfer films and wear debris.

Briscoe proposed that polymer wear falls into two categories known as cohesive wear and interfacial wear [8]. Briscoe describes cohesive wear as wear involving dissipation of frictional work such as abrasion and fatigue. The level of damage due to

sliding is prescribed by surface asperities and surface traction largely governed by the cohesive strength of the polymer. Briscoe describes interfacial wear as wear involving dissipation of frictional work by transfer and is more damaging than cohesive. He also points out that the current research indicated a correlation between wear rate and the reciprocal of the work to rupture ($1/\rho_y\varepsilon_y$) for a given polymer. Briscoe goes on to state that polymers considered ductile, such as PTFE, are far less affected by rough surface anomalies than glassy polymers such as PMMA, and that PTFE can accommodate more strain before rupture. He gives an equation for ductile abrasion based on a theory of asperity resistance:

$$\mu = \left(\frac{2}{\pi \tan \phi} \right) \tag{6}$$

$$z = \left(\frac{KW \tan \phi}{H} \right) \tag{7}$$

Where μ is the coefficient of friction, ϕ is the slope of a conical asperity, W is normal load, H is hardness, and K is probability constant. In regard to PTFE, Briscoe also points out that molecular orientation affects transfer wear, and that the transfer is largely unchanged polymer. Most polymers form a thick lumpy film during transfer. However, PTFE transfer is inconsistent forming either a relatively thin film or a patchy uneven film once steady sliding has occurred. There also appears to be an upper limit for sliding velocity at a given temperature for which transfer can occur. Briscoe also states cracking and delamination may be responsible for the transfer film often appearing “rumpled” and having patches of plate-like polymer removed from the film. He also states that this debris acts like a lubricant in the case of PTFE. To conclude, Briscoe points out the need

for continued research but suggests that wear rate is a function of the material and a dominant wear mechanism.

Briscoe [9] also investigated the effects of combined rotating and linear sliding motions on the wear and transfer of PTFE. Briscoe contends that the increasing wear of PTFE with increasing number of traverses is dependent on kinematics of relative motion between the sample and the substrate surface. Wear is dependent on sliding distance, and normally increases with increasing distance. For the vertical pin-on-disc machine shown in Figure 2.1 wear rate actually decreases with increasing number of traverses.

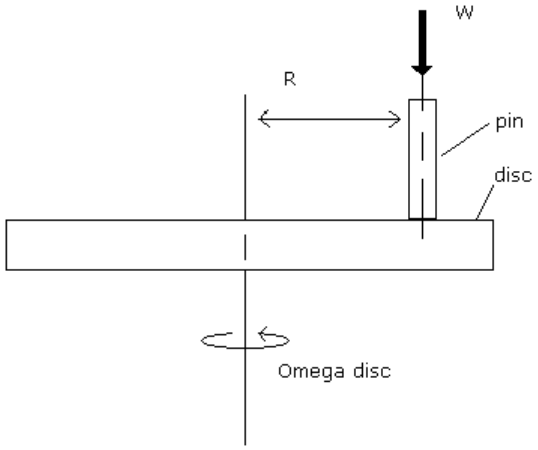

Figure 2.1. Vertical pin-on-disk configuration.

PTFE wear shows a behavioral change depending on the angular velocity of the pin. Effective linear sliding is achieved when the pin is rotated with the same angular velocity of the disc but in the opposite direction. Wear remains a function of sliding distance, but decreases as the pin's angular velocity is varied to simulate pure linear sliding to rotational sliding with a radius equal to the radius of the PTFE pin. Briscoe showed that the combination of spins inputs energy into the system that results in wear rate fluctuations. A relative rotation between the pin and disk inhibits molecular orientation

and results in increased wear and friction. Briscoe also states that motion aligned with polymer fibers leads to fibers being pulled away from the bulk.

Wear and friction of PTFE are known to undergo a transition at approximately 0.1 km. Vijayan and Biswas [10] observed a slight expansion in the unit cell up to this distance of sliding and unit cell shrinkage with increased sliding distance. They also observed a steady increasing in wear rate and friction until a steady-state wear and friction were reached around 3 km of sliding. They were also able to confirm that no change in the atomic structure of the PTFE surface took place over this distance. Although Vijayan and Biswas contend there is a strong correlation between wear rate and unit cell volume, they were unable to correlate the change in crystallite sizes to wear rate.

Brainard and Buckley [11] discovered that PTFE would transfer to metals under static conditions if a normal mass of 100 g were applied (pin dimensions not given). Due to the increased area of contact under load, it is not clear whether or not the transfer is load dependent. They also were able to conclude that PTFE transfer is possible with or without an oxide layer covering the metal substrate. Therefore, the chemical behavior of the substrate is not significant. The adhesion force was non-existent during the first two minutes of loading. Therefore, Brainard believes that adhesion is strongly influenced by creep.

2.2 Attempted Improvements in Wear Characteristics of PTFE

Cheng et al. [12] improved the wear properties of PTFE by preparing a composite with 60% wt. lead and 5% wt. glass fiber. Xue and Xie recorded friction coefficients and mass loss of PTFE composite samples sliding on steel using a pin-on-disc configuration with an oil lubricant. They concluded that PTFE containing modified glass fiber demonstrated better wear resistance and possessed a lower friction coefficient than virgin

PTFE. They credited the lead and glass fillers with decreasing wear by controlling the size and shape of the wear debris. The glass fiber also provides load support at the sample/substrate interface that decreases wear of the PTFE composite.

There have been several attempts to optimize the surface features of sliding counterfaces. Optimizing these features would achieve the lowest possible polymer wear and friction. Wieleba [13] studied the frictional and wear relationship between PTFE composites and the surface texture of steel counterfaces. While maintaining sliding velocity, pressure, and sliding distance constant throughout all tests, Wieleba carried out his experiments under dry sliding conditions. Using regression functions, Wieleba showed that wear rate is more dependent on surface features than friction. The regression functions predict that friction is most greatly influenced by the mean spacing between asperities. The larger the spacing between peaks the higher the friction value became. Wieleba suggests that large spacing makes formation of a PTFE transfer film more difficult. He showed friction was similarly influence by average asperity slope. The smaller the average slope the larger area of contact, consequently, adhesion forces friction to increase. Wear rate was most strongly influenced by asperity peak heights and the peaks' average radius of curvature. The higher the asperity peaks as well as the sharper the peaks the more severe the wear. This is explained by the increase in mechanical interactions between the counterface and the PTFE under such conditions. The combination of factors affecting wear and friction presented by Wieleba suggest that optimal tribological conditions will yield low wear in conjunction with low friction.

Jintang [14] proposed that PTFE forms metal fluorides during sliding contact with stainless steel. He claims extremely complex chemical reactions caused by compression, tension, and shear may take place and allow PTFE its solid lubricant attributes.

PTFE transfer is initiated when a polymer particle is removed from the bulk and adheres to the counterface. The particle then pulls the rest of the PTFE molecular chain from the bulk and eventually forms a film. Pleskachevsky and Smurugov [15] investigated the significance of thermal fluctuations on PTFE transfer film formation. They were able to show that the friction upon restart of a paused sliding test is dependent on the duration of the pause. After short pauses friction resumes the same as before the pause. As the pause duration increases the restart friction increases until it reaches the initial sliding value. Many researchers have suggested that the transfer film formation causes a drop in the friction value, however, after long pauses the polymer behaves as if there were no transfer film. Pleskachevsky and Smurugov suggest that the friction is more dependent on the PTFE/substrate interface temperature. They believe this explains the behavior of PTFE after pauses in sliding. They also observed that static and dynamic friction decrease with increasing test temperature. This is significant because there is no film transfer when static friction is occurring. Since both static and dynamic friction are affected, temperature can not be given credit for reducing friction by improving PTFE's self-lubricating properties. Pleskachevsky and Smurugov also show that test temperature becomes less significant as normal load increases. Other tests have shown that increasing load produces a thinner more efficient transfer layer.

After failing to produce an irradiated PTFE/unirradiated PTFE composite with wear properties favorable to unirradiated PTFE, Blanchet and Peng [16] were able

manufacture a composite PTFE/irradiated Fluoropolymer (FEP) with improved wear properties to PTFE. The composite contained 50% FEP irradiated to 30 Mrad and 50% unirradiated PTFE. Their experiments were run using a three-pin-on-disk configuration on a stainless steel counterface. They found the composite to wear considerably less and have a lower friction coefficient than PTFE under the same sliding conditions. The large plate-like wear debris commonly resulting from PTFE sliding is suspected to increase friction by adding to surface ploughing and deformation. The composite sliding yielded only thin oriented films. Blanchet and Peng suggest this is evidence that the wear debris morphology is indicative of friction. Also, the irradiated/unirradiated composite was non-abrasive to the steel counterface and possessed stronger creep resistance.

Sui [17] demonstrated that friction coefficient of a PTFE composite under sliding has a non-linear dependence on speed. The composites friction was lower at slow speeds than at high speeds. They also confirmed a strong dependence on contact stress. In order to avoid severe wear they determined sliding must take place at speeds less than 20 m/s along with contact stresses below 0.5 Mpa. Contact stress was shown to decrease while sliding after an initial run in period. The stress is believed to drop with increasing contact width.

PTFE wear rate data was collected from the aforementioned authors and is displayed in Table 2A below. Wear rates along with the major test parameters known to influence wear rate are displayed.

Table 2-1. Collection of PTFE wear rate data from previous authors.

Sliding in atmospheric conditions and room temperature

	Paper	Load (N)	V (m/s)	Distance (km)	Pin Geometry	Ra (um)	Counterface	K (mm³/Nm) Avg.	Publication
Pin - on - disk	Circular wear path								
	*[a] Tanaka et. al.	14.7	0.3	0.2	3 mm diameter		Glass	6.6E-4	The Mechanism of Wear of PTFE Wear, 23 (1973) 153-172
		14.7	0.3	0.4	3 mm diameter		Glass	6.0E-4	
		14.7	0.3	0.6	3 mm diameter		Glass	5.6E-4	
		14.7	0.3	0.8	3 mm diameter		Glass	5.6E-4	
		14.7	0.3	1.0	3 mm diameter		Glass	5.7E-4	
Pin - on - disk	Circular wear path								
	Tanaka et. al.	9.8	0.05	0.5	3 mm diameter		Glass	3.8E-4	
		9.8	0.05	1.0	3 mm diameter		Glass	2.2E-4	
		9.8	0.05	1.5	3 mm diameter		Glass	1.5E-4	
		9.8	0.05	2.0	3 mm diameter		Glass	1.2E-4	
		9.8	0.05	2.3	3 mm diameter		Glass	1.1E-4	
Pin - on - disk	Circular wear path								
	Tanaka et. al.	9.8	0.2	0.5	3 mm diameter		Glass	4.9E-4	
		9.8	0.2	1.0	3 mm diameter		Glass	4.8E-4	
		9.8	0.2	1.5	3 mm diameter		Glass	4.9E-4	
		9.8	0.2	1.75	3 mm diameter		Glass	4.9E-4	
	Circular wear path								Wear-Resistant PTFE via Electron Irradiation Lubrication Engineer 52, 6, 489-495
	Blanchet et. al.	104	0.05	5.5	4 mm X 4 mm	0.01	304 S. Steel	1.1E-3	
Pin - on - disk	Circular wear path								
	Blanchet et. al.	104	0.01	0.1	4 mm X 4 mm	0.01	304 S. Steel	9.6E-4	Wear Resistant Irradiated FEP / Unirradiated PTFE Composites Wear 214 (1998) 186-191
		104	0.01	0.2	4 mm X 4 mm	0.01	304 S. Steel	8.7E-4	
		104	0.01	0.3	4 mm X 4 mm	0.01	304 S. Steel	8.3E-4	
		104	0.01	0.4	4 mm X 4 mm	0.01	304 S. Steel	8.9E-4	
		104	0.01	0.5	4 mm X 4 mm	0.01	304 S. Steel	1.0E-3	
Pin - on - disk	Linear wear path								
	Briscoe et. al.	79.6	0.5	3.75	13 mm diameter	0.2	Mild Steel	7.6E-4	Transfer Wear of Polymers During Combined Linear Motion and Load Axis Spin Wear, 104 (1985) 121-137
		79.6	0.5	5.9	13 mm diameter	0.2	Mild Steel	9.7E-4	
		79.6	0.5	10.6	13 mm diameter	0.2	Mild Steel	7.5E-4	
		79.6	0.5	14.4	13 mm diameter	0.2	Mild Steel	7.5E-4	
Pin - on - disk	Circular wear path								
	[b] Briscoe et. al.	17.0	0.2	0.75	6 mm diameter	0.2	Mild Steel	1.2E-3	
		17.0	0.2	1.4	6 mm diameter	0.2	Mild Steel	1.3E-3	
		17.0	0.2	2.1	6 mm diameter	0.2	Mild Steel	1.3E-3	
		17.0	0.2	2.9	6 mm diameter	0.2	Mild Steel	1.2E-3	
		17.0	0.2	3.6	6 mm diameter	0.2	Mild Steel	1.3E-3	

* Test run in vacuum [a] Pre-rubbing of sample [b] Briscoe combined rotations

Briscoe, Evans, Pelillo, and Sinha [18] used a scratching technique to investigate the energies related to surface deformation of polymers. Their research focused on the characterizing wear and adhesion of polymers that produce thin transfer films including PTFE. They indicate that the elastic properties of polymers such as PTFE impart a restoring force to asperities that scratch the polymer surface, and that the nature of this mechanism is a minimization of energy dissipated for material displacement. They also indicate that PTFE experienced low levels of strain and responded elastically to a blunt indenter.

2.3 Wear of UHMWPE

In regards to ultra-high molecular weight polyethylene (UHMWPE), Wang [19] produced a theoretical wear model. Wang's theory originated from the observance of fibrils composing most of the wear debris, and the importance of multi-directional sliding on wear rate. Multi-directional sliding leads to shear and tensile stresses acting in concordance. Any molecular orientation in the direction of one motion has weak resistance to motion in another direction. Wang states that if enough energy is put into the UHMPE surface a fibril may be pulled from neighboring fibrils. The work of friction must act perpendicular to the fibril alignment in order for wear to take place. Wang also states that there exists a critical value of coefficient of friction below which fibril removal will not occur. There also exists a critical cross-link density above which fibril removal will not occur.

While improving the wear resistance of UHMWPE, crosslinking has also resulted in a decrease of material toughness. Muratoglu [20] investigated the crosslinking effects on UHMWPE's wear behavior with a pin-on-disk tribometer. They demonstrated that there was a linear relationship involving molecular weight between crosslinkings and wear rate. Muratoglu's findings agree with previous findings that wear rate decreases with increasing crosslinking density. They also state that crosslinking affects the polymers ability to orient its molecular chains while sliding. Therefore, crosslinking improves wear behavior under multi-directional sliding.

In their review of current concepts in wear of total hip and knee replacements, Schmalzried and Callaghan [21] state that polyethylene wear is different from creep. Creep deforms the polyethylene but does not produce any wear particles. Oxidation reduces the ability of irradiated UHMWPE to form crosslinks between molecular chains.

Therefore, oxidized UHMWPE suffers from higher fatigue rates and delamination. UHMWPE wear is also highly sensitive to scratches on the counterface surface. Wear rate increases thirty to seventyfold when scratches of two micrometers in depth are present [21].

Wear tests by Burroughs and Blanchet [22] in 2000 showed that shelf-aged irradiated UHMWPE was less wear resistant than melt (200°C) vacuum post-irradiation storage by approximately three-fold. The shelf-aged irradiated UHMWPE displayed wear similar to unirradiated UHMWPE under multi-directional sliding against polished surfaces. They also demonstrated that under multi-directional sliding UHMWPE does not undergo the initial run-in wear period observed during unidirectional sliding. Given the motion present in hip and knee joints, behavior during multi-directional sliding is of more concern than unidirectional sliding. The tests run by Blanchet and Burroughs consist of circular motion tests and rectangular motion tests. The wear rates for both these forms of testing proved comparable. This suggests that multi-directional motion of any kind is sufficient to produce higher wear than unidirectional motion.

Suh [23] presented the delamination theory of wear in 1973 for metals. The theory is centralized around the assumption that subsurface material cold-works more than material near the surface due to a greater dislocation density in the subsurface. Cold working causes cracks to develop in the subsurface that eventually join together. When the cracks reach a critical length the material between the crack and the surface will shear and wear debris is thus produced. Suh also states that the same wear mechanisms are responsible for adhesive and fatigue wear. Although this theory was developed for metals, Briscoe [8] later indicated that delamination might play a role in polymer wear.

PTFE wear debris morphology appears in a plate-like form that is characteristic of delamination. Delamination is driven by subsurface shear stresses that are not influenced by the direction of sliding only that sliding exists.

CHAPTER 3
ENGINEERING APPROACH

3.1 Six-Station Pin-on-Flat Tribometer

The objective of this project was to elucidate some of the wear mechanisms associated with load fluctuation and multi-directional motion of special polymers (PTFE). Testing was performed using a pneumatically load controlled six-station pin-on-flat tribometer developed at the University of Florida (UF) and presented in the thesis by Aaron Ison. Several PTFE wear tests were performed using the six-station test rig prior to commencement of this project to confirm the validity of this device as a tribometer. The test rig was equipped with linear voltage differential transducers (LVDT) in order to confirm translation and position of the movable stage. Load cells were used to verify that the pneumatic pressure devices supplied the intended load to the samples. The results of the preliminary testing indicate that the tribometer offers motion and load control accurate enough for this project.

3.1.1 Table and Drive System

The six-station tribometer was designed to provide a means of creating multi-directional motion while allowing in-situ variable load capabilities. The sample counterfaces were translated using a multi-axis drive system. The system consists of a stage set atop two linear tables stacked on top of one another and configured in a perpendicular alignment. The top table is translated by a linear microstepper while the stage is translated along the top table by another linear microstepper. This allows the

stage to travel anywhere in a horizontal x – y plane. A controller manages the position, motion, velocity, and acceleration of the tables. Programs describing the motion path are sent from a computer to the controller's local memory. The controller then determines the necessary signals needed to produce the desired motion and sends them to the microsteppers.

3.1.2 Pneumatic Control

Six pneumatic cylinders are used to apply normal load to the polymer samples. Pressure is supplied at 1.3 MPa by a 120 gallon compressor and is regulated by two 0 – 207 kPa pressure gauges. These pressure gauges can be seen in Figure 3.1 below.

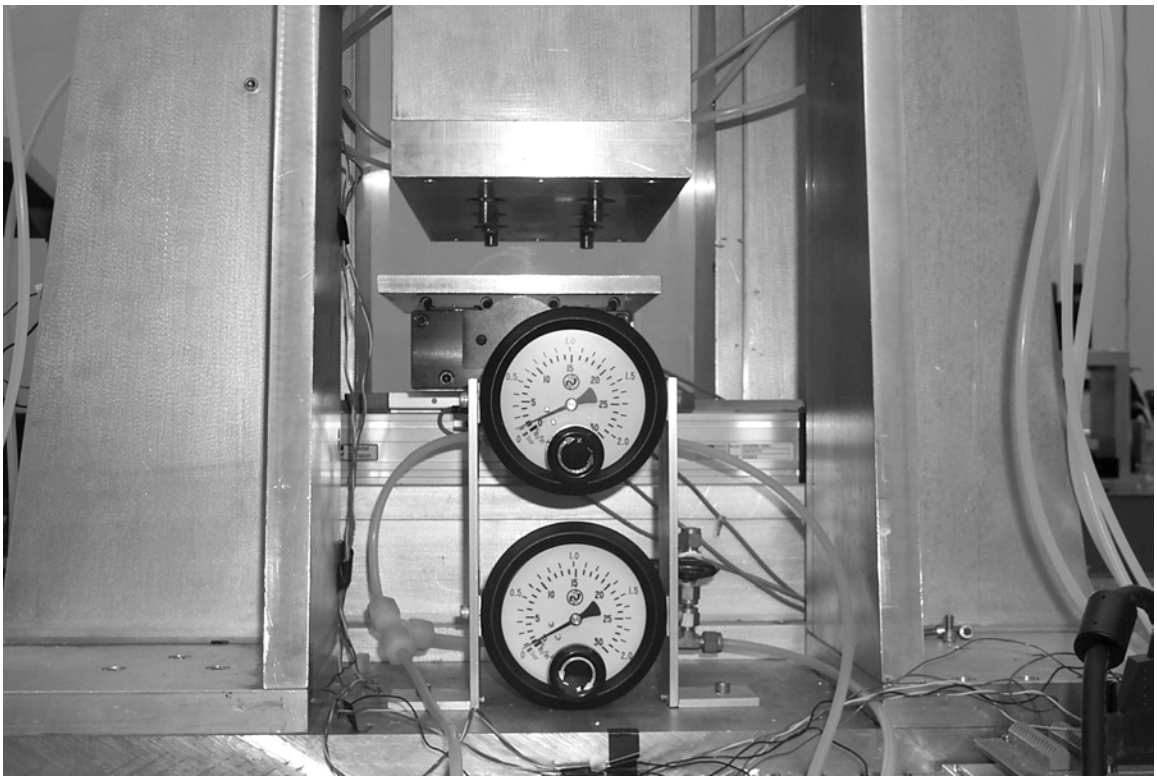

Figure 3.1. Photograph of pressure gauges (top) backpressure to cylinders (bottom) pressure to electro pneumatics.

The top mounted pressure gauge supplies backpressure to the cylinders as a means of separating the polymer samples from the counterfaces. The bottom pressure gauge supplies air to six electro-pneumatic pressure transducers. Each electro-pneumatic is

connected to one of the six pneumatic cylinders, and can supply pressure ranging from 0 – 138 kPa. A 0 – 5 Vdc signal sent to the electro-pneumatics controls the pressure supplied to the cylinders. The electro pneumatic arrangement can be seen in Figure 3.2.

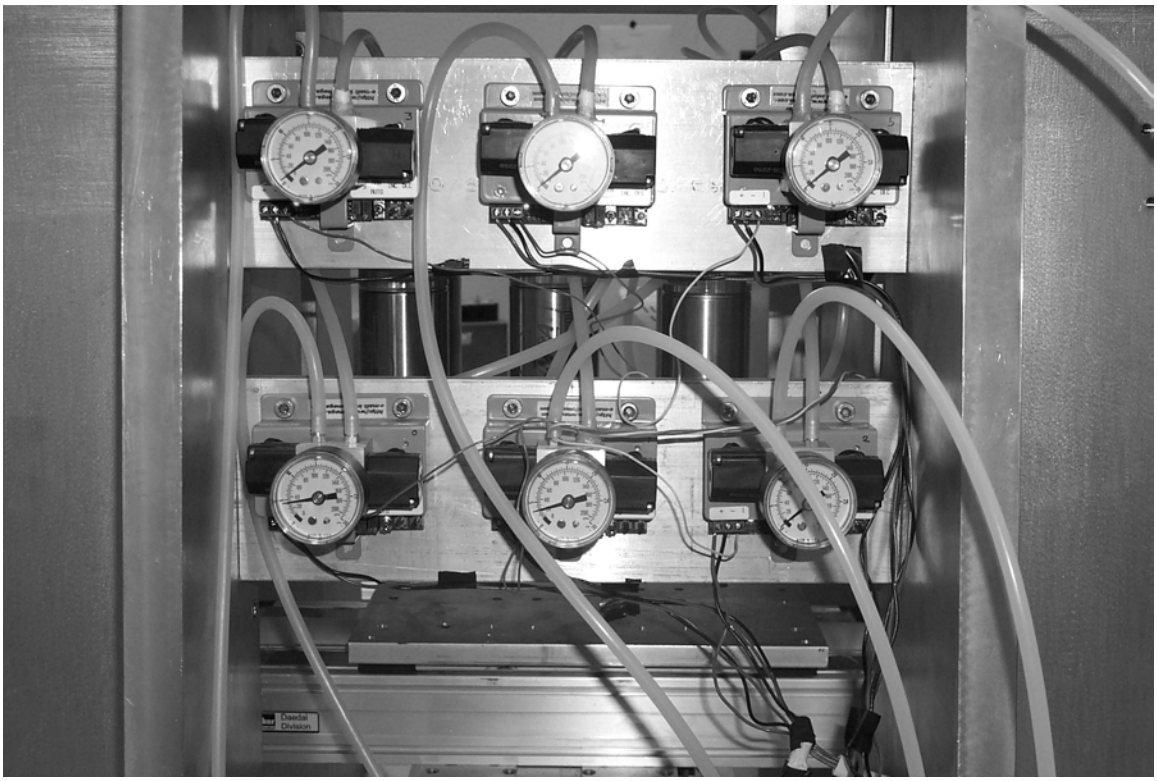

Figure 3.2. Arrangement of electro pneumatic gauges.

The output pressure is linearly proportional to the voltage supplied. Each electro-pneumatic is controlled independently by separate signals sent from a computer that can either be programmed to fluctuate or hold constant. For all the tests presented in this paper, the pressure supplied to the electro-pneumatics was held constant at 207 kPa. Voltage signals ranged from 0 – 5 V depending on desired test parameters, and were used to produce output pressures ranging from 0 – 138 kPa sent to the cylinders. The signals can be manipulated to model any desired loading pattern within the limits of the electro-pneumatic pressure range and time response.

The pneumatic cylinders are all aligned perpendicular to the movable stage in two rows of three. The arrangement can be seen in Figure 3.3.

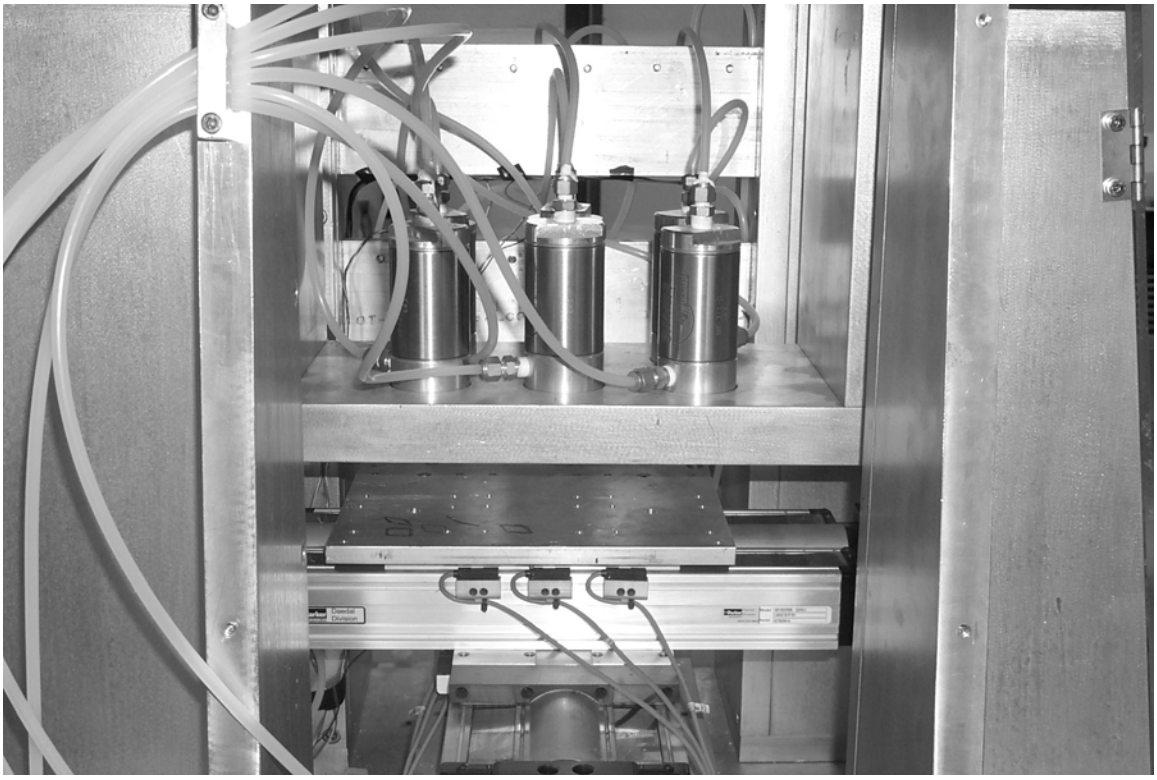

Figure 3.3. Photograph of pneumatic cylinder arrangement.

The cylinders possess a 2-inch inner diameter and have a threaded stem used to attach the polymer sample holders. Each cylinder can apply a maximum load of 68 lbs (293 N) directly to the polymer samples. An illustration showing the entire pin-on-flat tribometer is displayed in Figure 3.4. Finally, the equipment log detailing the components needed to operate the tribometer is displayed in Table 3-1.

3.1.3 Sample Holders

Six polymer sample holders were machined out of stainless steel to provide a rigid brace for the polymer samples. The sample holders were designed specifically for use with the pneumatic cylinders and can be viewed in Figure 3.5. A shop drawing of the sample holder can be viewed in Appendix C.

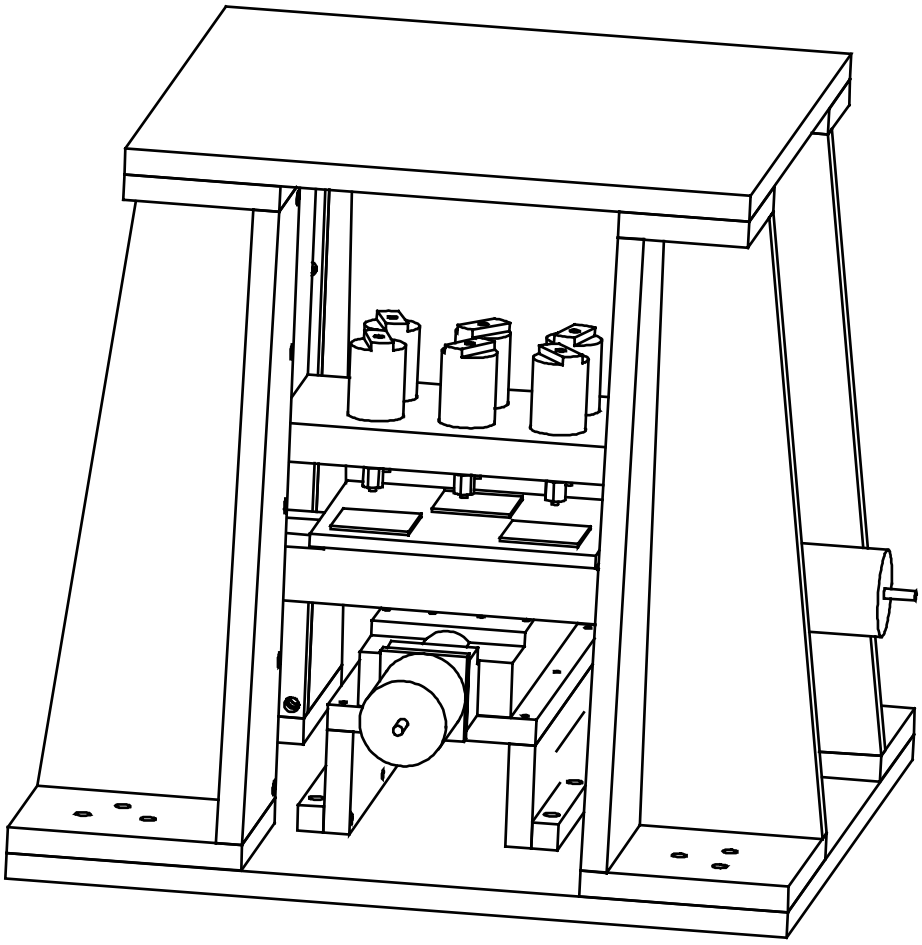

Figure 3.4. Assembly drawing of entire pin-on-flat tribometer.

Table 3-1. Equipment register for pin-on-flat tribometer.

Equipment	Manufacturer/Supplier (Product Number)	Quantity	Description
Linear Table	Parker Automation (406100XRMS)	2	Square rail bearing with linear screw
Amplifier	Parker (Compumotor) (OEMZL4)	2	Amplifier for use with motors
Pressure Gauge	Omega (PRG501-30)	2	Regulate supply pressure to electro pneumatics
Indexer/Drive Cable Motors & Motor to	Parker (Compumotor)	2	8 Amp drive microstepper used to translate counterfaces
Load Cell	Omegadyne (LCKD-100)	3	Signle-axis load cell for measuring normal load
Connector Block	National Instruments (SCB-68)	1	Allows computer to collect data from tribometer
Conditioner	Omega (DP25-S)	3	Condition voltage signal form LCKD-100 to load
Power Supply	Omegasnap (DRN-PS-1000)	2	Convert wall voltage to 24 Vdc signal @ 850 mA to power electropneumat
Daq Board Cable	National Instruments (SH68-68-EP)	2	Communication between computer and data aquistion boards
Daq Board	National Instruments (PCI-6034E)	1	Analog Input board for data collectior
Indexer	Parker (Compumotor) (6K8)	1	8 axis indexer drive
Pneumatic Cylinder	Bimba (NR-311-D)	6	Provide normal load ranging from 0 - 63 lbs to the samples
Connector Block	National Instruments (CB-68LP)	1	Allows computer to send data to tribometer
Daq Board	National Instruments (PCI-6713)	1	Analog output board for controlling electro pneumatics
Electro Pneumatic Transducer	Omega (IP413-020)	6	Provides active control of supply pressure to cylinders

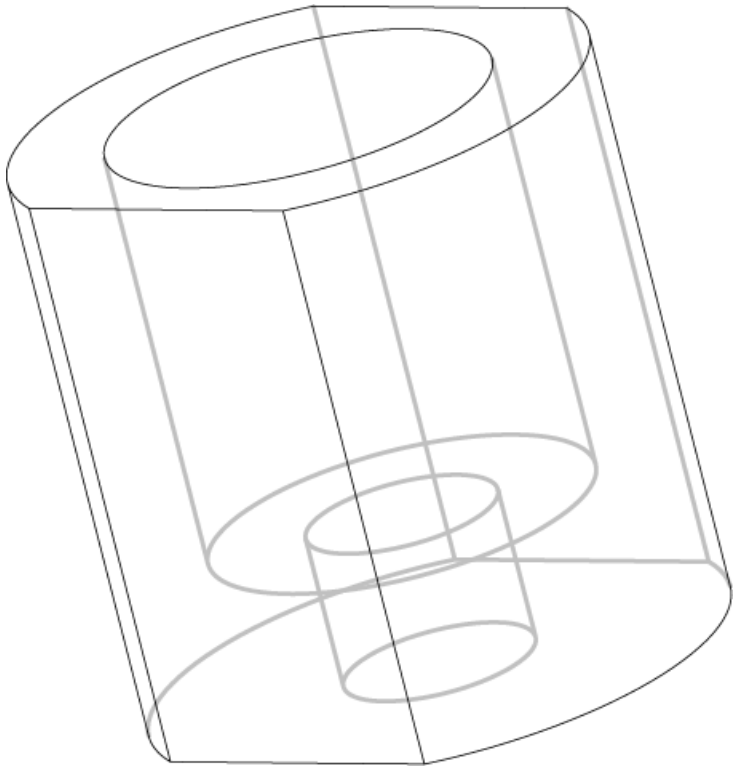

Figure 3.5. Schematic of polymer sample holder.

The sample holders consist of a ½ inch inner diameter tapped to fit the cylinder stems with a ¼ inch thru hole cut through the centerline. The ½ inch diameter runs ¾ inch deep and bottom shelf flattened by an end-mill. The ¼ inch hole is cut through the shelf and is ¼ inch deep. The large diameter end of the polymer sample fits snuggly inside the sample holder with the polymer stem extending through the ¼ inch hole. The ¼ inch hole allows the polymer to contact the counterface and lends side support to the polymer stem during sliding. The sample holders are numbered along with the cylinders for bookkeeping purposes.

3.2 Motion Paths and Loading Patterns

All sliding tests were performed in air under several motion paths and loading patterns. The first motion path consisted of simple linear reciprocating through a stroke

length of 40.6 millimeters and an average sliding velocity of 46.5 mm/s. This motion was used for several wear tests and in each case ran for 4 hours producing a sliding distance of 670 meters. For the first series of tests all six cylinders were held at constant pressure. The test pressures at the cylinders were 56, 84, and 112 kPa corresponding to loads of 117, 176, and 235 N respectively. These loads equate to nominal pin pressures of 3.69, 5.56, and 7.42 Mpa. The second series of tests consisted of the same motion path, but applied loads oscillating at 6 second cycles. The range of load oscillation was different for each test. The first test oscillated from 148 – 206 N the second 117 - 235 N and the third 59 – 295 N. Each of these tests had an average load of 176 N. Finally a third group of tests consisting of a random selection of load peaks and valleys cycling once every 110 seconds was run with this motion path. The loading spectrum used in this test was modeled after a rain-flow spectrum presented by J. A. Collins [26], but was modified to achieve an average load of 176 N. A graph of the loading spectrum is shown in Figure 3.6.

A second linear reciprocating motion path was used to provide the longest possible stroke length that could be performed with the current counterfaces. The path ran diagonal to the rectangular counterface with each stroke spanning a distance of 63.5 millimeters. Again, the test ran for 4 hours but was operating at a sliding velocity of 48 mm/s and a total sliding distance of 690 meters. The loading used for this test was held constant at 176 N.

Three diamond patterns with varying degrees of crossing were also used as motion paths. The first diamond path ran at 30° of crossing with lengths of 16.6 millimeters.

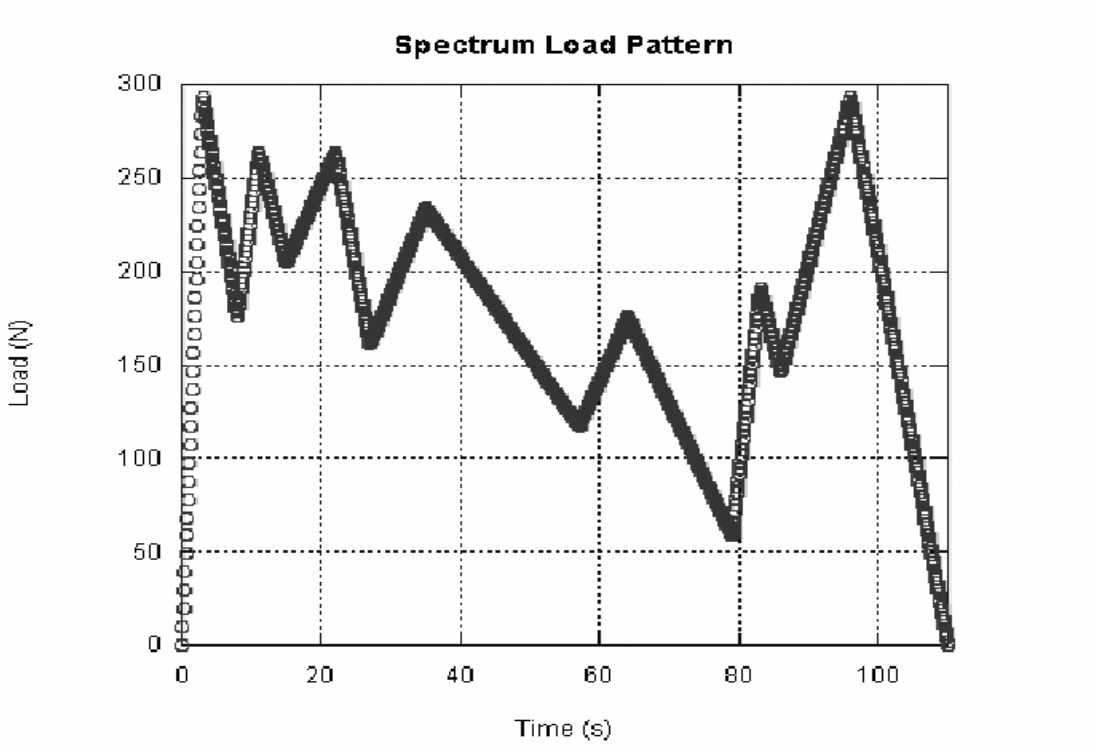

Figure 3.6. Loading spectrum applied to samples for wear testing.

The second diamond path ran at 60° of crossing with lengths of 16.2 millimeters, and the third diamond path ran at 90° of crossing with lengths of 15.8 millimeters. All of the diamond pattern tests were run for 4 hours with all six cylinders at a constant load of 176 N. The path lengths were calculated to match the wear path areas for all diamond patterns to the diagonal reciprocating test. The change in length of the diamond sides is due to the increase in the polymer pin's wear path area contribution. Due to the pin's circular geometry, an increase in degree of crossing causes an increase in wear path area whenever a change in sliding direction takes place.

Finally, five circular motion paths were generated with different diameters. Each test was run at a sliding velocity of 50 mm/s for 4 hours resulting in a sliding distance of 720 meters. For each of the five circular motion paths tested, all six cylinders were functioning with constant loads being applied to the polymer samples. However, the load

was different from cylinder to cylinder. In groups of two, the cylinders applied loads of 117, 176, and 236 N respectively. The diameters for the five circle patterns were 6.35, 10.6, 15.0, 25.4, and 36.4 millimeters respectively. Figure 3.7 displays the motion paths described in this paper.

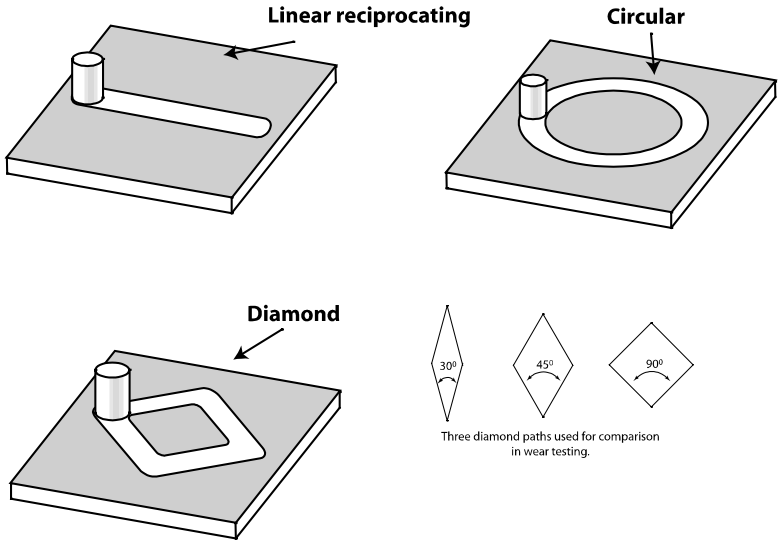

Figure 3.7. Motion paths used for wear testing.

The programs used to generate these motion paths are located in Appendix A.

3.3 Counterface Preparations and Handling

The counterfaces were cut from 440 stainless steel bar stock. Counterface material was chosen to provide a significantly harder surface than that of the polymer sample. Due to the high hardness of 440 stainless steel (Rockwell 54 C), wear of the counterface could be neglected while sliding against the much softer polymer samples (PTFE 58 R, UHMWPE 63 Shore D). The bar stock was cut into 6 rectangular plates 3 X 2.75 X 0.125 inches. The counterfaces were then prepared by a series of polishing steps as described in Table 3B., beginning with 220 grit sandpaper and ending with a 0.3 μm particle slurry.

Table 3-2. Polishing steps for raw counterface samples.

Step	Materials	Method
1.	220 grit SiC sandpaper	Polishing wheel
2.	440 grit SiC sandpaper	Polishing wheel
3.	600 grit SiC sandpaper	Polishing wheel
4.	15 μm particle slurry with billard cloth	Polishing wheel
5.	5 μm particle slurry with billard cloth	Polishing wheel
6.	1 μm particle slurry with embry cloth	Polishing wheel
7.	0.3 μm particle slurry with embry cloth	Polishing wheel

After polishing, the counterfaces were washed using water and a mild detergent then rinsed with methanol. Finally the surfaces of the counterfaces were characterized using an optical profilometer. Based on data collected from the profilometer the polishing technique described above yields an average surface roughness of approximately 0.02 μm. Following each wear test, the counterfaces were washed with water and detergent then polished, cleaned, and characterized using the steps described in Table 3C.

Table 3-3. Polishing steps for used counterface samples.

Step	Materials	Method
1.	5 μm particle slurry with billard cloth	Polishing wheel
2.	1 μm particle slurry with embry cloth	Polishing wheel
3.	0.3 μm particle slurry with embry cloth	Polishing wheel

Each of the six stainless steel counterfaces are constrained to the movable stage by four 4-40 facets, and are numbered to correspond with the cylinders and sample holders.

3.4 Polymer Sample Preparation

The PTFE samples were cut from molded ½ inch rod stock of virgin Teflon. Receiving coordinate information from the G – code presented in the appendix of this paper, the samples were cut using a CNC – mini – milling machine. A schematic of the

polymer sample can be viewed below in Figure 3.8 or a shop drawing can be viewed in Appendix C.

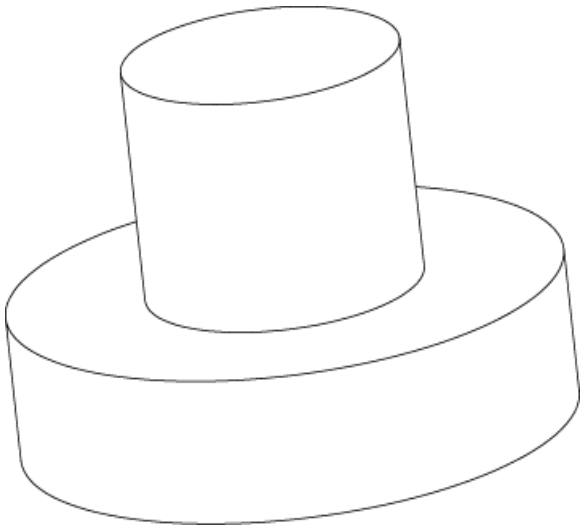

Figure 3.8. Schematic of polymer sample.

The polymer sample has a large diameter base of ½ inches and is approximately ¼ inches in thickness. The stem has a smaller diameter of ¼ inches and extends 2/5 inches from the base. Allowing the stem to extend 2/10 of an inch from the sample holder. The milling machine ensures that the base shelf and the stem's top surface are parallel to each other. The sample's base shelf sits flat against the inner surface of the sample holder. The sample's stem extends through the hole cut in the sample holder to contact the counterface surface. The sample is locked into position when the sample holder is threaded onto the cylinder. The UHMWPE samples were cut in the same manner and with the same dimensions as the PTFE samples. The unirradiated UHMWPE was cut from 1-inch stock samples 3/8 inch in diameter. The irradiated UHMWPE was cut from the interior of a shelf aged puck shaped sample. Prior to each wear test, the samples were placed in their respective sample holders and weighed individually. Once the wear test was completed, loose debris was removed from the polymer stem. The samples would

remain inside the sample holders as they were weighed. Mass loss during the wear test could then be calculated and used to determine wear rates.

CHAPTER 4
EXPERIMENTAL RESULTS

4.1 Electro-Pneumatic Performance Data

Load cell data collected to evaluate the performance of the electro-pneumatics is displayed in Figure 4.1.

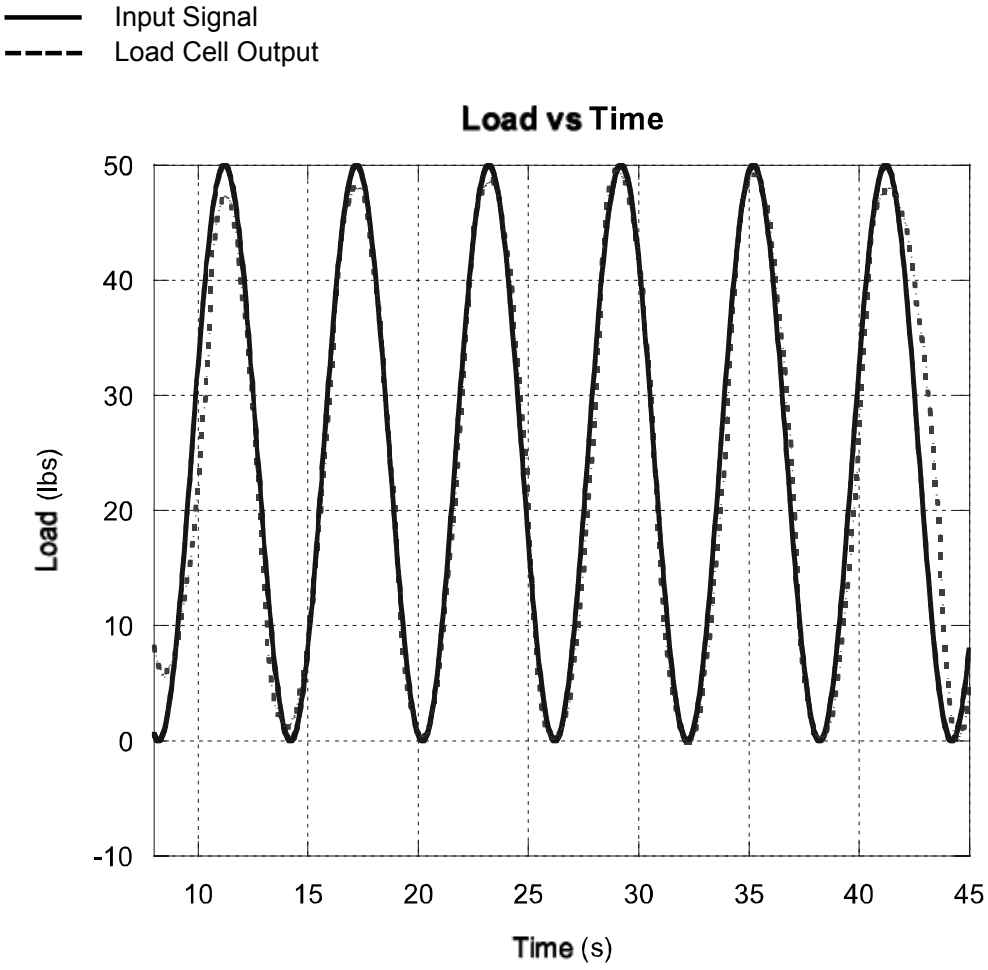

Figure 4.1. Electro-pneumatic performance data output from load cells.

The electro-pneumatics demonstrate the ability to follow a sinusoidal loading cycle that ranges from 0 to 80 % of maximum pressure and cycles once every 6 seconds. The

conditioners used to translate data received from the load cells were not capable of handling frequencies over 0.333 Hz. Therefore, there was inconclusive evidence regarding the electro-pneumatics ability to follow a 3 second cycle that spanned 0 to 80 % of the max pressure range. To ensure reliable testing parameters, all dynamic loading tests performed were constrained to frequencies equal to or below 0.167 Hz.

4.2 Variations in Wear Rate and Sliding Conditions

Along with the respective sliding conditions, the wear rates from every PTFE wear test performed are shown in Table 4-1. The raw data collected for these calculations can be viewed in Appendix B.

4.2.1 Transfer Film Formation

Although the tests involving PTFE were fairly consistent, data outliers occasionally appeared in the results. Out of the 93 tests run, where mass loss was the measured quantity, only 5 data points varied by more than 1 standard deviation from the mean for that test. The outlier appeared as an unexpectedly high wear rate 2 times, and appeared as an unexpectedly low wear rate 3 times. Unwaveringly, the appearance of outliers corresponded with two very distinct transfer films. Under reciprocating motion, high and normal wear always corresponded with the transfer film shown in Figure 4.2. The film appeared patchy and uneven with portions of the counterface still exposed. The patches appeared to be drawn out in the direction of sliding, but vary in width and length. Some patches even appeared to be deposited on top of a previous patch. In contrast, low wear always occurred in conjunction with the appearance of the smooth transfer film shown in Figure 4.3.

Table 4-1. Raw data with calculated wear rates.

Wear Path		Load	Wear Rate (mm^3/Nm)					
Reciprocating		Constant						
Test	Area (in^2)	Newtons	1	2	3	4	5	6
1	0.4491	117	3.47E-4	2.08E-4	3.64E-4	1.56E-4	2.49E-4	1.79E-4
2	0.4491	176	5.32E-4	5.05E-4	4.74E-4	4.85E-4	4.43E-4	3.93E-4
3	0.4491	235	5.43E-4	3.21E-4	5.43E-4	5.49E-4	5.61E-4	5.11E-4
Oscillating (Avg. 176 N)								
4	0.4491	147-205	4.93E-4	4.32E-4	5.74E-4	5.24E-4	5.09E-4	4.74E-4
5	0.4491	117-235	3.78E-4	4.05E-4	4.35E-4			
	0.4491	59-293				4.32E-4	4.74E-4	4.66E-4
Reciprocating Spectrum (Avg. 176 N)								
	Area (in^2)							
6	0.4491		6.24E-4	6.36E-4	6.05E-4	6.86E-4	6.70E-4	5.90E-4
Circular								
	Area (in^2)	Constant (N)	1	2	3	4	5	6
7	0.1963	117	1.51E-4	1.02E-4				
	0.1963	176			1.86E-4	2.33E-4		
	0.1963	235					2.69E-4	2.55E-4
8	0.3267	117	1.34E-4	1.51E-4				
	0.3267	176			3.08E-4	2.08E-4		
	0.3267	235					2.58E-4	3.60E-4
9	0.4625	117	2.42E-4	2.26E-4				
	0.4625	176			3.76E-4	2.94E-4		
	0.4625	235					3.95E-4	3.60E-4
10	0.7854	117	4.25E-4	3.87E-4				
	0.7854	176			4.66E-4	4.59E-4		
	0.7854	235					4.33E-4	5.89E-4
11	1.125	117	3.71E-4	3.01E-4				
	1.125	176			4.77E-4	5.31E-4		
	1.125	235					4.52E-4	5.59E-4
Semi-Circular								
	Area (in^2)							
12	0.4491	117	3.60E-4					
	0.4491	176			4.10E-4			
	0.4491	235						4.39E-4

Wear Path Diamond Test	Area (in^2)	Load 176 Newtons Included Angle	Wear Rate (mm^3/Nm) 1	2	3	4	5	6
13	0.6741	0	5.39E-4	5.50E-4	6.02E-4	5.39E-4	5.65E-4	5.91E-4
14	0.6741	15	7.03E-4	6.73E-4	6.82E-4	7.07E-4	6.82E-4	6.44E-4
15	0.6741	30	6.18E-4	5.97E-4	5.97E-4	6.22E-4	6.09E-4	6.05E-4
16	0.6741	45	4.66E-4	4.44E-4	4.44E-4	4.78E-4	4.40E-4	4.32E-4

Although these transfer films displayed regions of light and dark patches that appeared to run in the direction of sliding, there is no gross exposure of the underlying counterface. Unlike the high and normal wear films, the low wear films appeared very smooth and even. However, the regions of light and dark patches most likely indicate regions of varying thickness within the transfer film.

The wear debris associated with both kinds of transfer films are plate-like in geometry with most of the longer debris strips folded in an accordion fashion. However, the wear debris appeared slightly smaller under low wear than it did under high wear.

Another glairing contrast between the two films is the extension of transfer film over the wear path. For all reciprocating motion tests, the wear path consists of a long portion of constant width capped by semi-circular portions at both ends. In cases of high and normal wear, the transfer film extended only over the long portion of the wear path and large amounts of wear debris were deposited at the end points of the wear path. Whereas low wear transfer films cover the entire wear path.

Transfer films would also appear for circular sliding motion. However, the long drawn out patches that appeared during high and normal wear under linear reciprocating motion were now assembled into circular patches with diameters approximately equal to the width of the wear path. The transfer films were all consistent in appearance and no

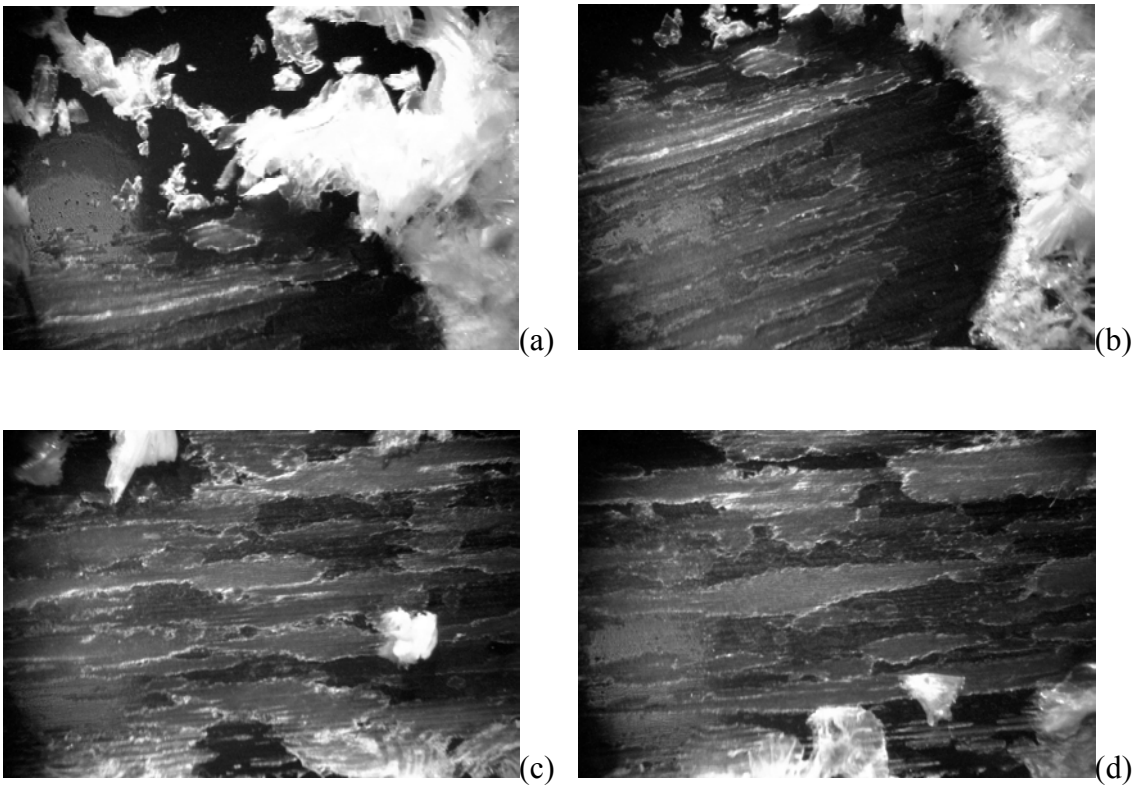

Figure 4.2. Optical micrograph of PTFE transfer film characteristic of high wear rates (a) wear debris (b) end of wear path (c) top middle (d) bottom middle.

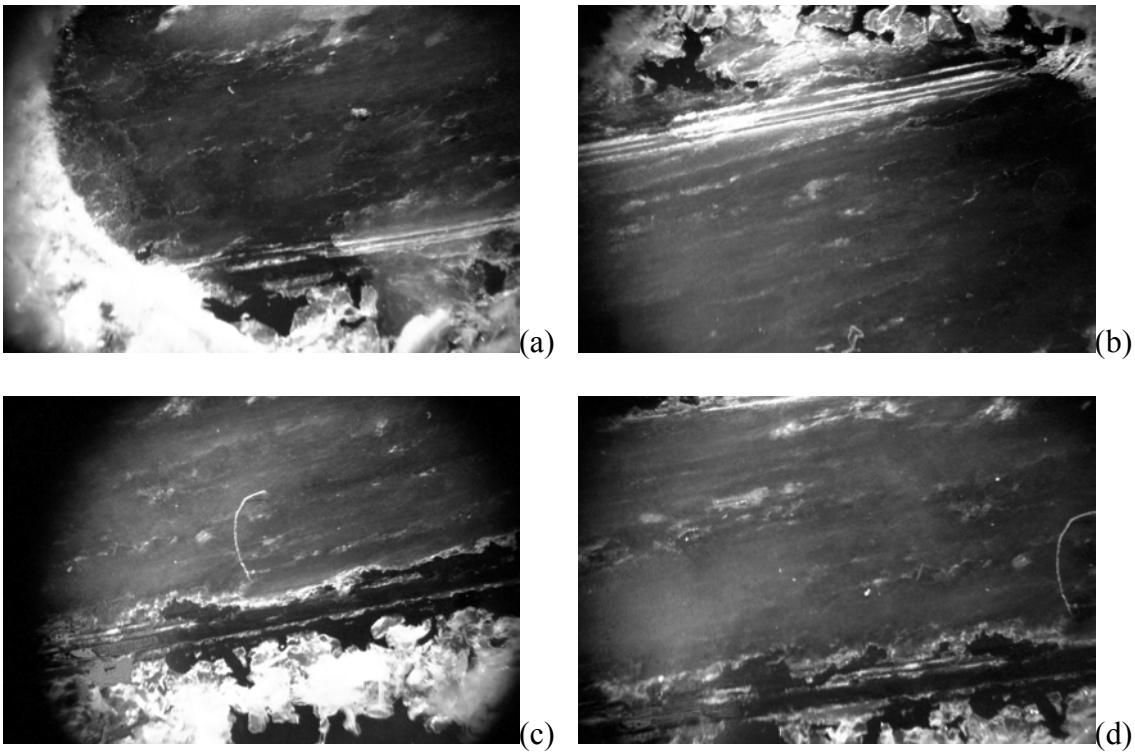

Figure 4.3. Optical micrograph of PTFE transfer film characteristic of low wear rates (a) end of wear path (b) top middle (c) bottom middle (d) middle.

major difference could be observed in the wear debris. Several images of circular motion transfer films can be seen in Figure 4.4.

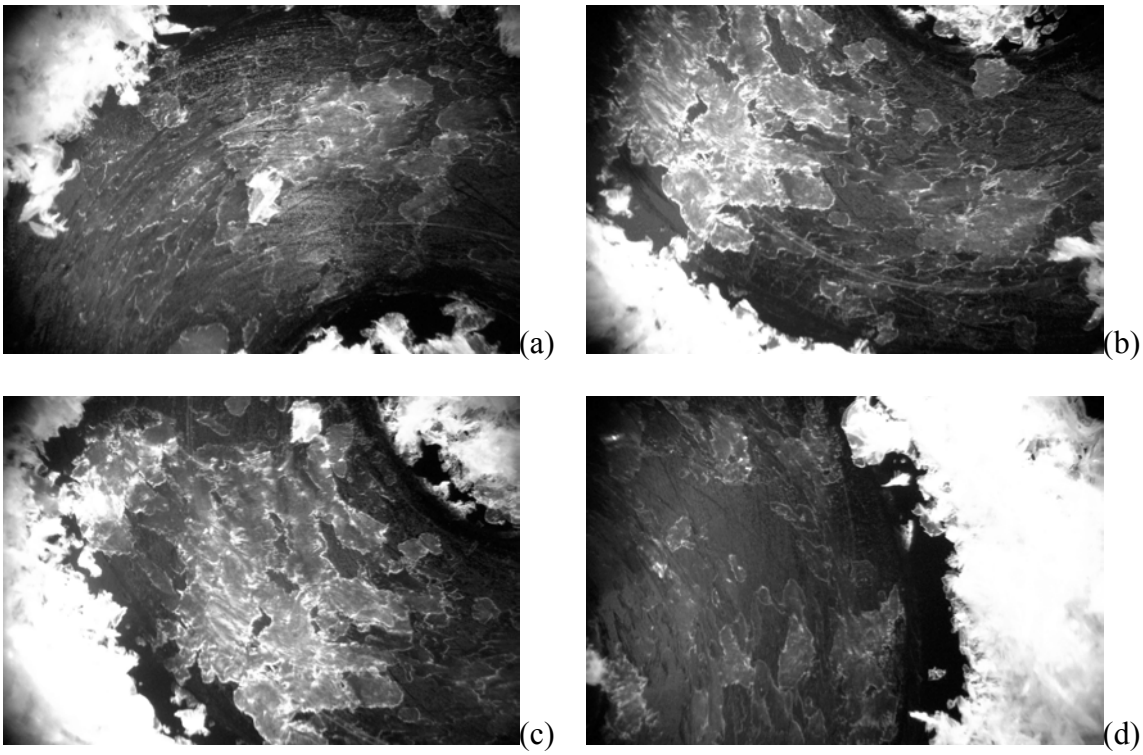

Figure 4.4. Optical micrograph of PTFE transfer film deposited by 14.9 mm diameter circular wear path (a) top (b) bottom (c) left (d) right.

Finally, images of the diamond motion transfer films are displayed in Figure 4.5. These transfer films possessed characteristics resembling that of linear reciprocating along the sides, meaning that the transfer film is consistent and appears drawn out in the direction of sliding. At the corners, motion comes to a stop then restarts in a different direction. This change in sliding direction is similar to what the polymer pin experienced at the end points of the linear sliding tests. At all the corners the transfer film appeared to breakup and deposit itself as small irregular shaped patches with sections of the counterface exposed. Large amounts of the plate-like wear debris observed in previous tests were deposited at the corners. Although the morphology of the transfer film

appeared different from the circular sliding tests, the wear debris showed no appreciable difference from either the circular or linear sliding tests.

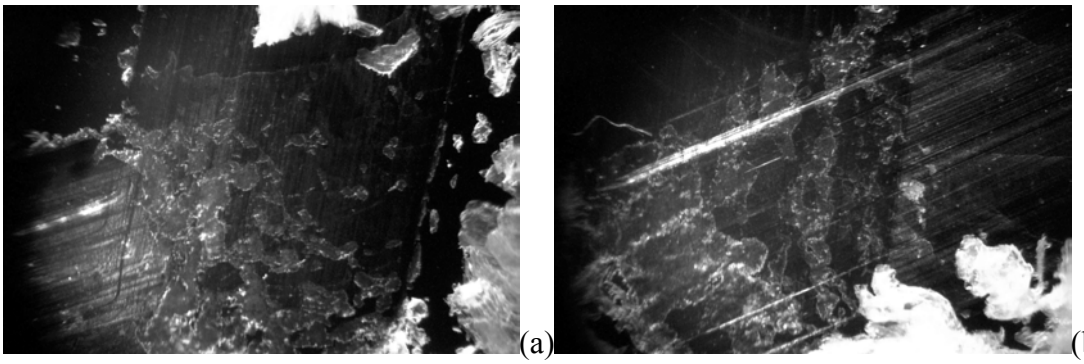
(a) (b)

Figure 4.5. Optical micrograph of PTFE transfer film deposited by diamond pattern (a) soft corner (b) sharp corner.

4.2.2 Wear Rate Comparisons

Comparisons between several wear tests are shown in Figures 4.6, 4.7, 4.8, 4.9, and 4.10 respectively. The volume of material lost during a wear test, v, was calculated by dividing the sample's mass loss by its density. The wear rate, k, was then calculated by dividing the volume loss by the total sliding distance and the average normal load applied during the test as shown in equation 8.

$$k = \frac{m}{\rho s d} \tag{8}$$

Figure 4.6 shows the variation in wear rate as load increases under linear reciprocating sliding motion. Each data point represents a sample slid for 670 meters under constant load. The data shows an obvious trend that wear rate is proportional to load, but variations in wear rate for each load do exist. At 117 N, the wear rate varied from 1.56E-4 to 3.64E-4 mm^3/Nm with a standard deviation of 35 percent. The average of all six samples was 2.5E-4 mm^3/Nm. With the exception of a single outlier at 235 N, the wear behavior is more consistent at 176 and 235 N with standard deviations of 10 and 18 percent, and average wear rates of 4.72E-4 and 5.05E-4 mm^3/Nm respectively.

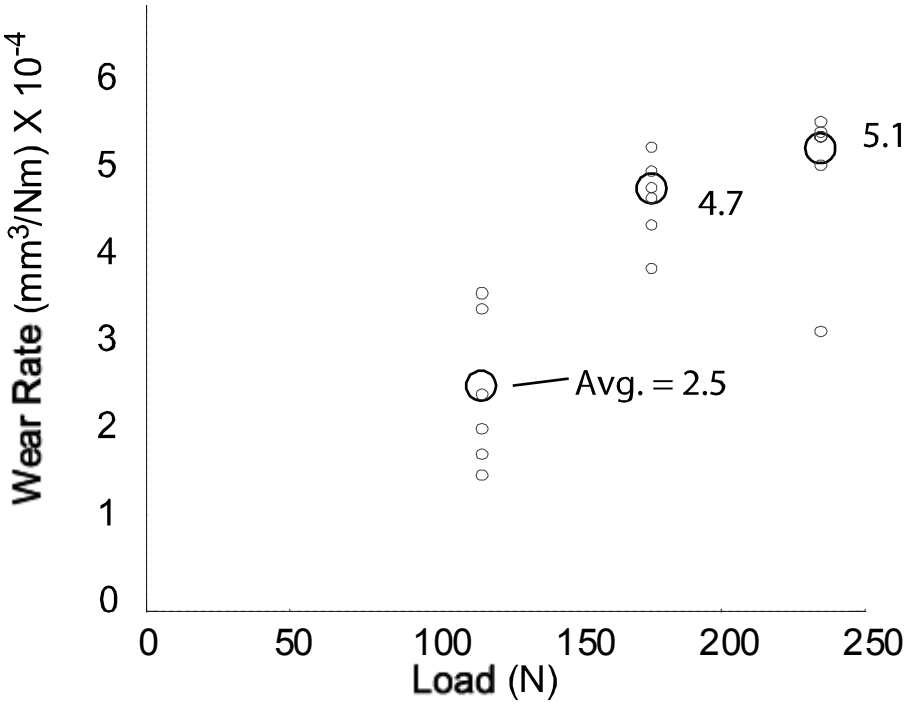

Figure 4.6. Wear rate as a function of load for 670 meters of linear reciprocating sliding. The proportionality of increase in wear to increase in load for identical motion paths is similar to data presented by Tanaka [1].

For the same reciprocating wear path and sliding distance, data presented in Figure 4.7 indicates that oscillating load does not produce any change in wear behavior from that of constant load. Regardless of the magnitude of oscillation, the wear rates remained comparatively close to previously reported wear rates produced under a constant load equal to that of the oscillating load's average value. The average wear rates were 5.01E-4 for 58 N of oscillation, 4.06E-4 for 118 N of oscillation, and 4.57E-4 mm^3/Nm for 234 N of oscillation. However, wear rates for the loading spectrum shown in Figure 3.6 of the Engineering Approach section of this paper were significantly higher than those produced with a constant load averaging 176 N. The average wear rate of all six samples was 6.35E-4 mm^3/Nm. The load fluctuations in Figure 3.6 act at nearly the same

frequency as those applied in the oscillating load test, however, the loading is more heavily weighted at the beginning of the cycle.

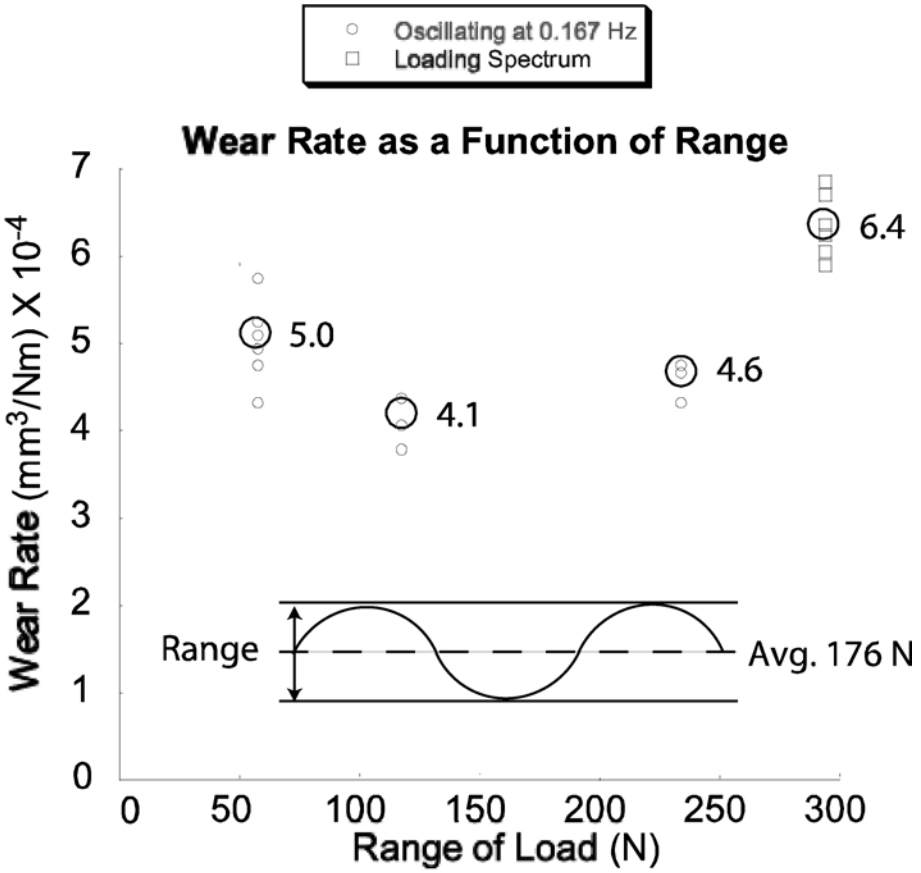

Figure 4.7. Effects of varying load on wear rate compared with effect of loading spectrum on wear rate.

Following the progression of wear rate and load shown in Figure 4.6, the wear results for spectrum loading more closely resemble those expected for a constant load of 293 N. A load of 293 N was applied for brief moments during the spectrum test. For the samples used in this test, 293 N of load borders on exceeding the yield strength of the material and may have altered the material's wear behavior.

Figure 4.8 shows the effect of diameter on the wear rate for samples slid 720 meters in a circular motion path. As with reciprocating motion, the three constant load values were applied. Each test indicated that wear again increased with increasing load.

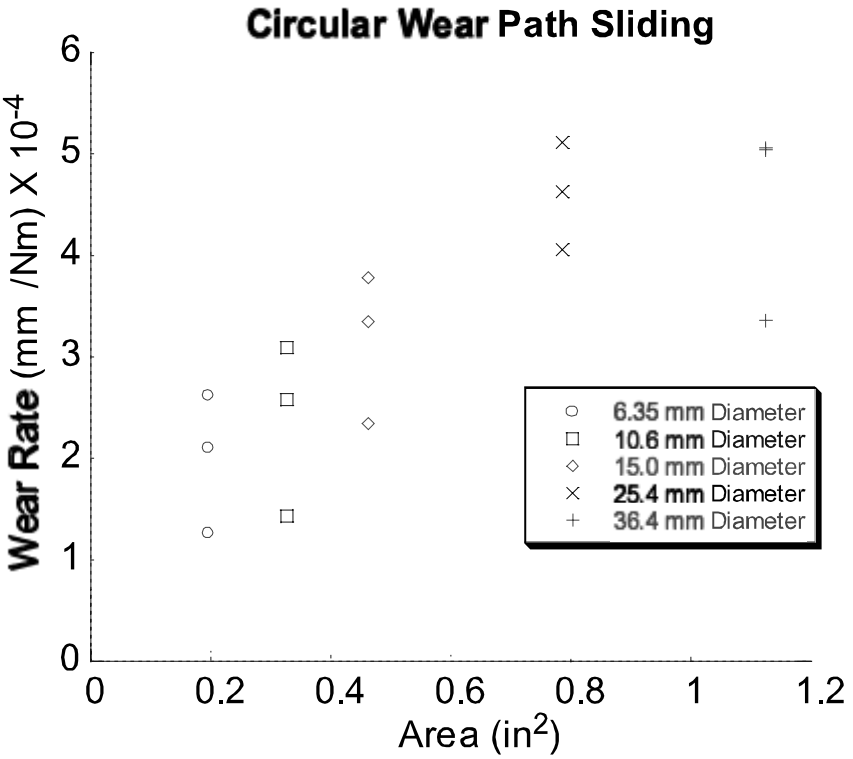

Figure 4.8. Effects of load and diameter on wear rate for circular motion.

An overall view of the circular motion tests indicated that wear increased at a fairly linear rate with increasing diameter. This behavior agrees with data presented by Briscoe [9] and what was expected given the increase in wear path area. Although Tanaka [1] provided data showing higher wear rates for smaller diameter circular wear paths, the tests loading and sliding speed were not identical. The only exception to the increasing wear with increasing diameter trend presented in this paper appears for the 36.4 mm diameter test when the wear rate decreased for 117 and 235 N loads from the 25.4 mm diameter test. All circular motion tests were preformed at the same sliding velocity. Therefore, the number of cycles increased with decreasing diameter. For tests with the same wear path area, wear rate proved to be higher under linear reciprocating motion than it did for a circular motion path. As can be seen in Figure 4.9, the wear rate for

circular sliding motion does not become equal to that of linear sliding motion until the circular wear path area is nearly 1.75 times greater than the linear wear path.

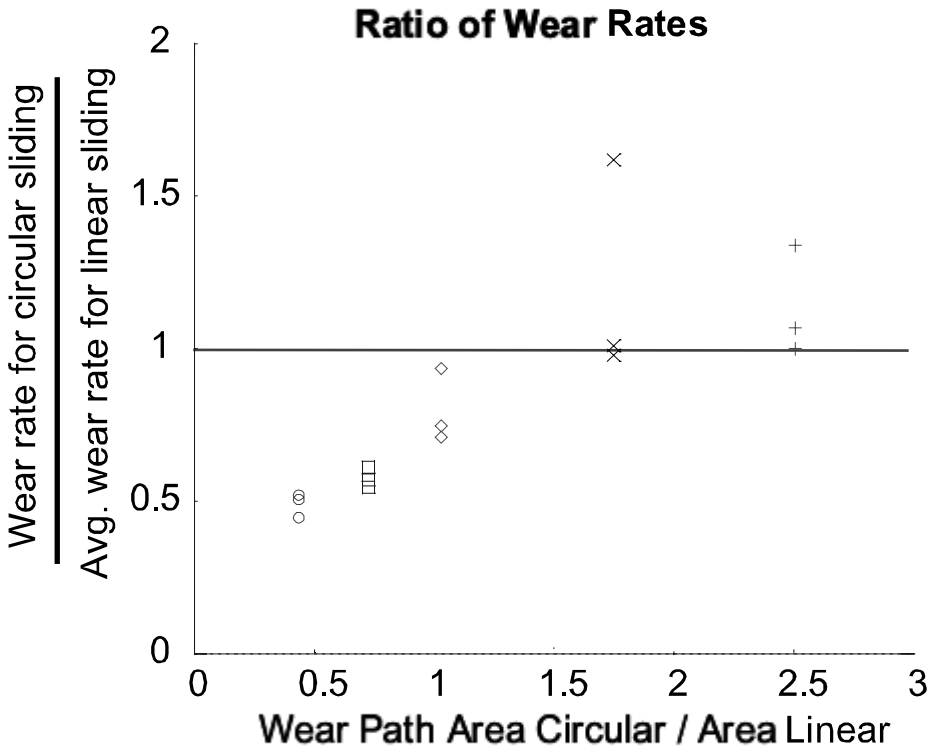

Figure 4.9. Ratio of circular motion wear rates over linear reciprocating motion wear rates.

The wear rate ratios were calculated by taking the average wear rate from a circular motion path of given diameter and dividing that value by the average wear rate from linear reciprocating motion of the same load. The area ratios were calculated by determining the wear path area of a given diameter test and dividing that value by the wear path area created from a single pass under linear reciprocating motion. Although this data is consistent with findings by Briscoe [9], increasing wear with increasing diameter is in contrast to what was expected given the current theories regarding polymers such as UHMWPE and multi-directional sliding. However, this trend may be explained by the increasing number of cycles incurred by the polymer pin with decreasing wear path diameter and assuming a directional independent wear mechanism.

Figure 4.10 shows the change in wear rate as a function of the angle of inclusion for several diamond shaped wear paths. All of the diamond pattern tests were run with a constant load of 176 N for a total of 4 hours. Due to changes in the motion path from test to test, the total sliding distance for 0° angle of inclusion differed from the other tests. The 0° angle of inclusion test slid for 695 meters while all other tests slid for 621 meters. The distances correspond to sliding speeds of 48.3 and 43.1 mm/s. Despite the small difference in speed, it is important to note that the higher sliding speed may result in an increase in wear relative to lower sliding speed tests. However, it is safe to assume that whatever change in wear rate resulted from different sliding speeds, it is not significant enough to produce a change in any trend observable in Figure 4.10. For 0° angle of inclusion the six samples had an average wear rate of 5.64E-4 mm^3/Nm. The average wear rate at 15, 30, and 45° of inclusion were 6.82E-4, 6.08E-4, and 4.51E-4 mm^3/Nm respectively. Although there was excellent consistency in the data from each set of tests, standard deviations of 4.78, 3.29, 1.74, and 3.88 % respectively, there was no consistency in the wear behavior from test to test. Wear rate increased from 0° to 15° of inclusion then decreased slightly at 30° of inclusion and finally decreased sharply at 45° of inclusion. With the exception of the 45° angle of inclusion, the wear rates collected under diamond shaped sliding motion were higher than any other wear test run with the same load. The wear path area was 4.35 cm^2 for all four tests. This wear path was 1.5 times greater than the wear path created under the previous linear reciprocating motion tests. However, wear rate was only shown to increase by this much when 15° of inclusion was incurred, and at 0° of inclusion wear rate increased by only 1.2 times that of the previous linear reciprocating tests.

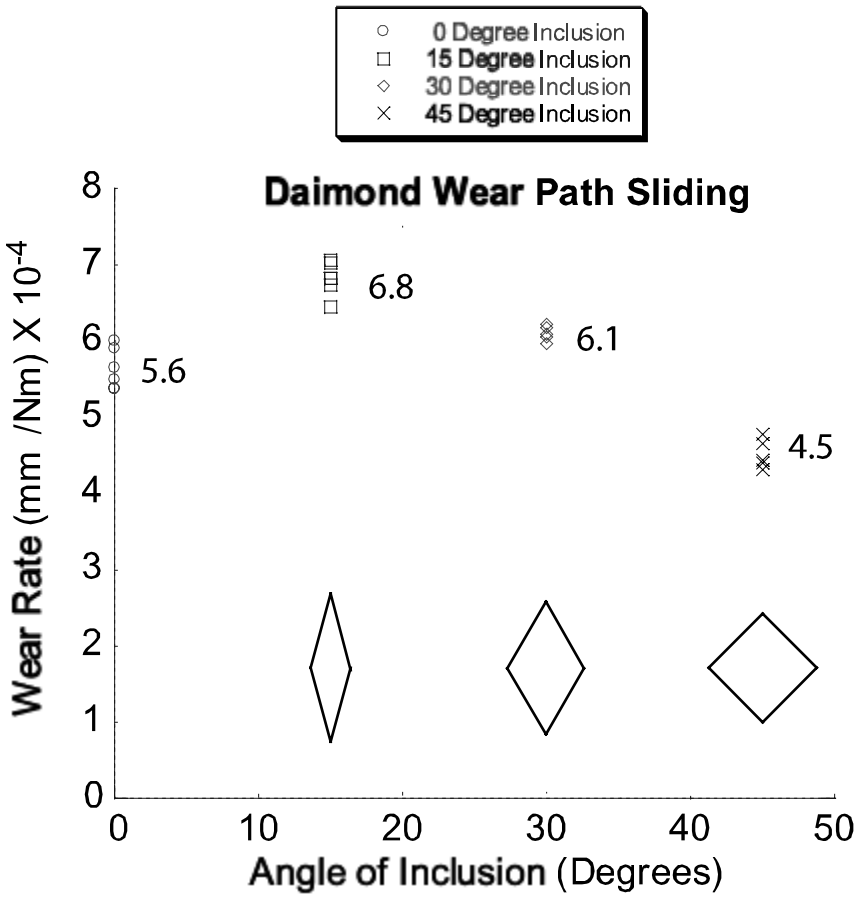

Figure 4.10. Wear rates for diamond pattern sliding motion as a function of inclusion.

4.3 Cycle dependence on Wear

Wear rate shows an inverse dependence when plotted against the number of cycles incurred during sliding as shown in Figure 4.11 below. Regarding circular path wear tests, the least number of cycles run was approximately 8000 and corresponded to the highest wear rate for any such motion. As the number of cycles increased, the wear rate asymptotically approached some value around 0.18 x $10^{\wedge -3}$ mm^3/Nm. A similar trend appeared with the linear reciprocating and diamond path tests. Although the wear rates for this group were generally shifted up from the circular path wear curve, the final data point at 52000 cycles fell below what was expected from the circular path wear curve.

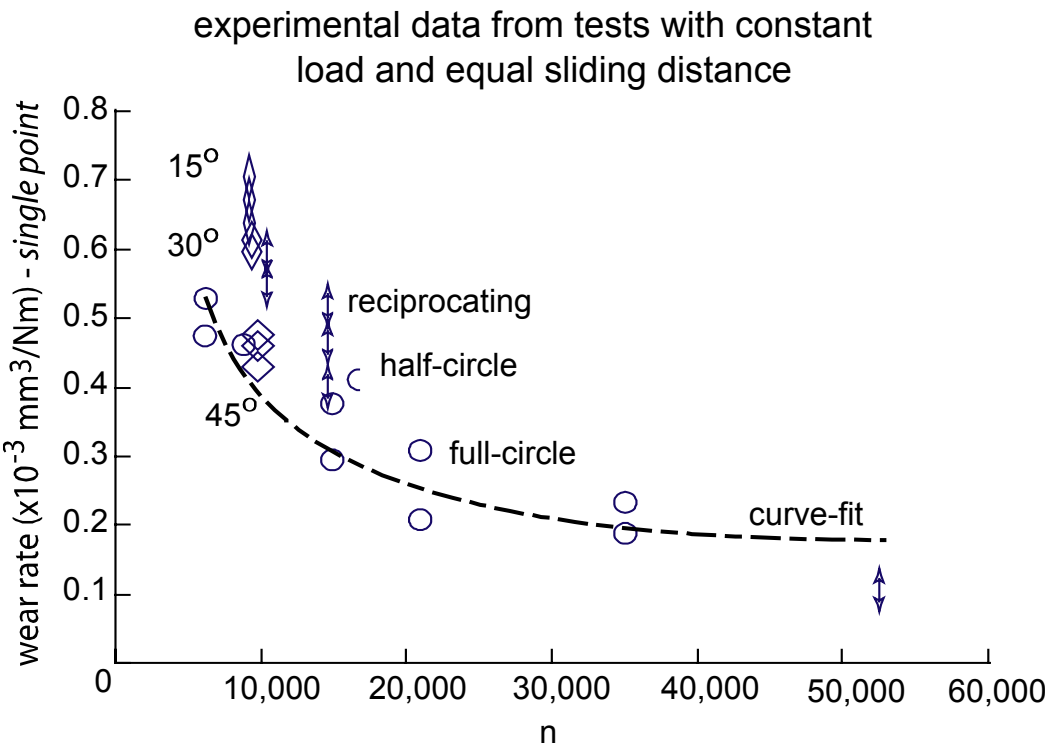

Figure 4.11. Wear rate as a function of number of cycles.

4.4 Images of Wear

An image of the polymer samples before and after wear testing can be seen in Figure 4.12.

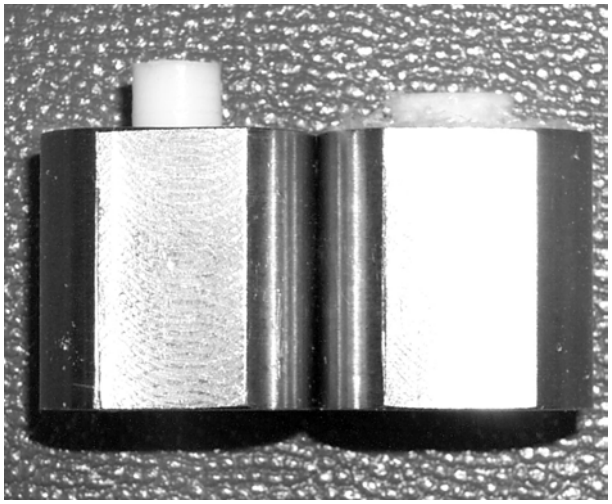

Figure 4.12. Photograph of polymer samples before 4 hour linear reciprocating wear test at 176 N (left), and after (right).

The amount of PTFE wear resulting from different loads after being ran for 720 meters at 50 mm/s in a circular sliding motion of diameter 36.4 mm can be seen in Figures 4.13 and 4.13. Figure 4.13 shows the sample holders marked 0 and 3 run at 117 N, holders marked 2 and 5 run at 176 N, and holders 1 and 4 run at 235 N.

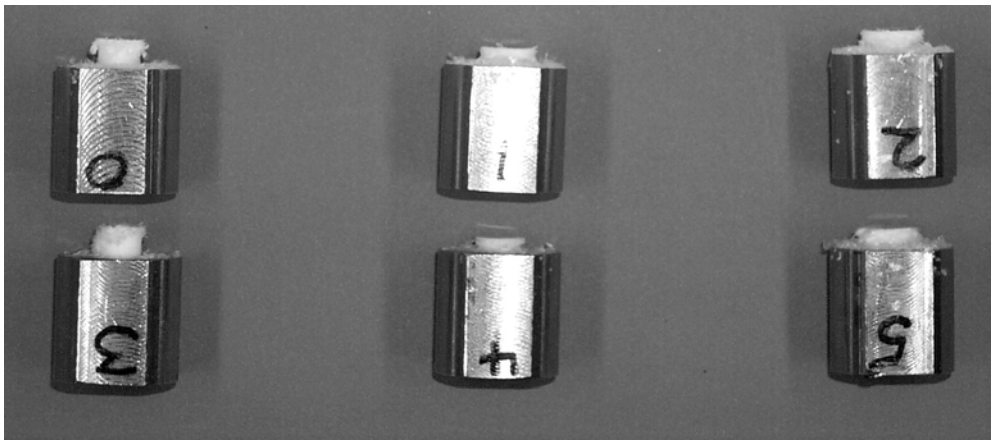

Figure 4.13. PTFE wear post 720 meters slid testing at 50 mm/s. Left 117 N, middle 235 N, right 176 N.

Figure 4.14 shows the PTFE wear paths resulting from the same test.

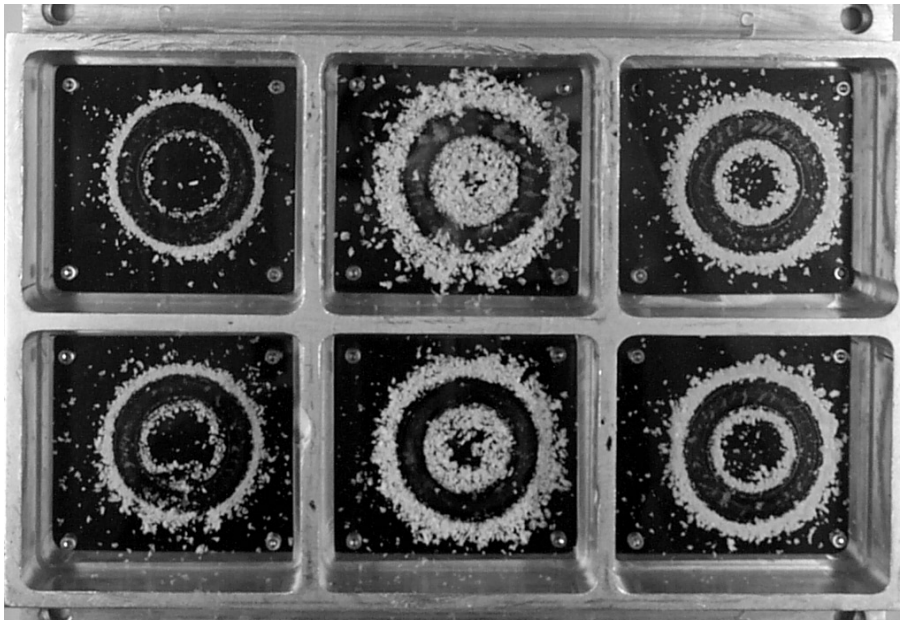

Figure 4.14. Wear paths post 720 meters slid testing at 50 mm/s. Left 117 N, middle 235 N, right 176 N.

CHAPTER 5
SURFACE CHARACTERIZATION AND SUBSURFACE STRESS MODELING

Based on data collected from optical stylus scans of the steel counterface prior to wear testing, the surface was assumed to be sinusoidal in nature with a 40 nm amplitude and a 30 μm period. The optical scan information supporting these numbers is shown in the appendix of this report. The scan filtered out data with frequencies higher than 100 cycles per millimeter. This frequency was iteratively chosen because it gave a roughness value approximately equal to the average roughness of the entire counterface while eliminating any sharp asperities that would not actually support a significant amount of the normal load. The asperity density was modeled by assuming the pit-centered configuration shown in Figure 5.1.

The area per asperity peak was calculated using equations 9 and 10.

$$\lambda = \frac{\beta}{\sqrt{2}} \tag{9}$$

$$\psi = \lambda^2 \tag{10}$$

Where ψ is the counterface area per asperity peak and λ is the length of one side of the square shown in Figure 5.1 above. The number of asperity peaks in contact with the polymer pin at any time was calculated using equation 11.

$$\Omega = \frac{A_p}{\psi} \tag{11}$$

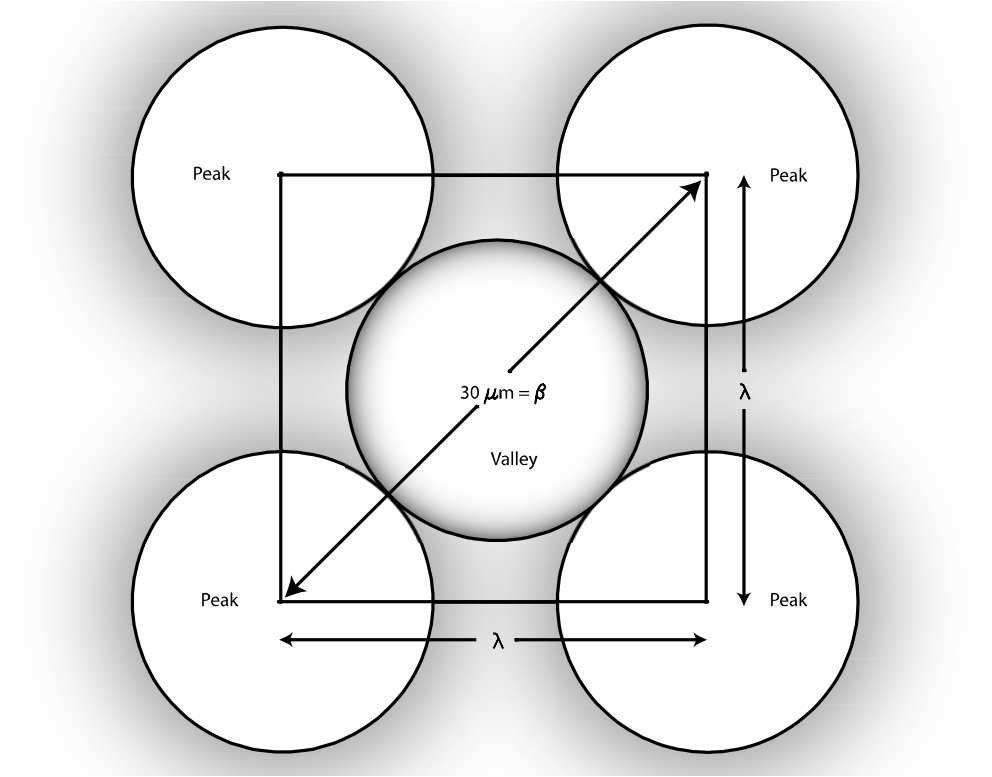

Figure 5.1. Asperity peak configuration at the surface of the steel counterface.

Where Ω is the number of asperity peaks in contact with the polymer pin and A_p is the area of the pin face. Once the number of asperity peaks in contact with the pin is known the load per peak, f_{asp}, can be calculated by dividing the normal load by the number of peaks Ω. The peak radius, Rcp, shown in Figure 5.2 can be calculated before determining the Hertz elastic contact patch by using equation 12.

$$R_{cp} = \frac{1}{2}\left[\frac{c^2}{4 \times h} + h\right] \tag{12}$$

Assuming that the polymer surface is identical to the counterface surface, the composite radius becomes

$$R = \frac{R_{cp}}{2} \tag{13}$$

R can now be used with the Hertz contact patch equations to determine the size of the

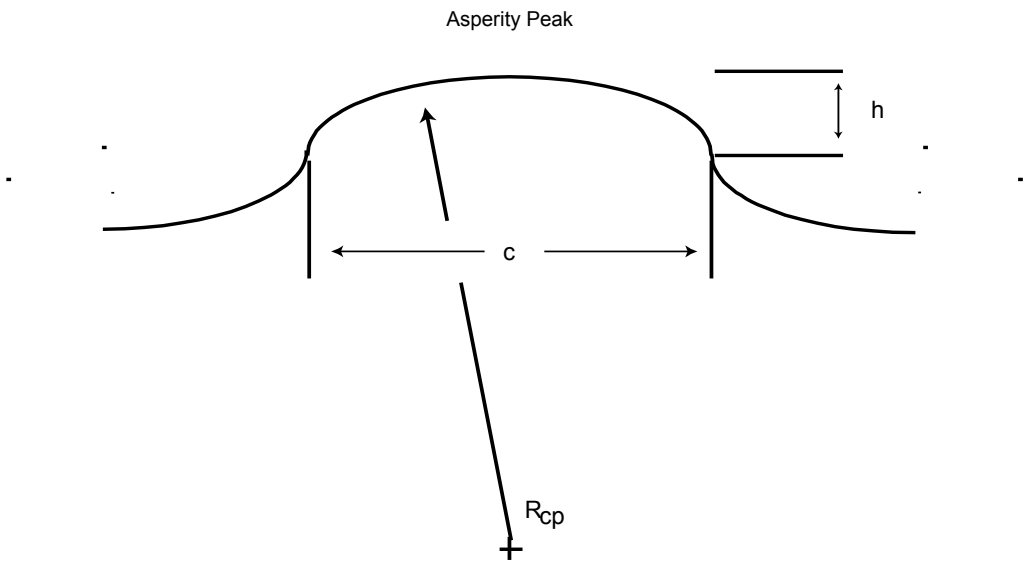

Figure 5.2. Radius of asperity peak at surface of steel counterface.

contact patch between the polymer and counterface.

$$a = \left(\frac{3 \times f_{asp} \times R}{4 \times E'} \right)^{\frac{1}{3}} \tag{14}$$

Where a represents the radius of a circular contact patch and E' is the composite modulus of elasticity for steel and PTFE. R was shown to be orders of magnitude larger than the contact patch therefore confirming the Hertzian contact assumptions. The maximum pressure is then calculated using equation 15.

$$P_{\max} = \left(\frac{3 \times f_{asp}}{2\pi a^2} \right) \tag{15}$$

The pressure profile along the surface of the polymer pin is shown in Figure 5.3. Given the low friction value between PTFE and steel, distortion of the pressure profile can be neglected once sliding has occurred [27]. The equation describing the pressure profile shown in Figure 5.3 is substituted in place of P(s) in the stress equations for an elastic half-space 16,17,18.

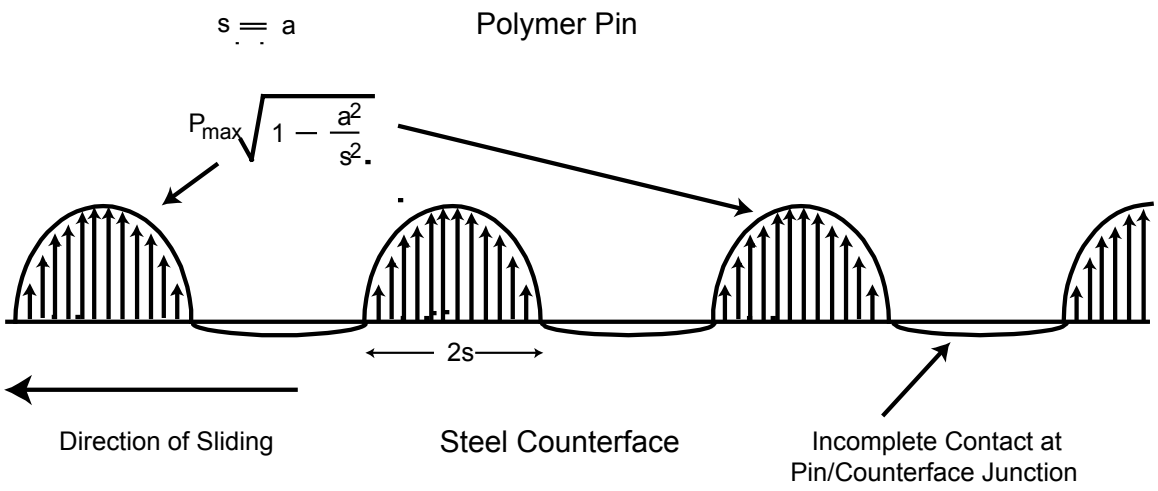

Figure 5.3. Pressure profile applied to PTFE surface when in contact with counterface.

$$\sigma_x = -\frac{2z}{\pi}\int_{-a}^{a}\frac{P(s)(x-s)^2}{\left\{(x-s)^2+z^2\right\}^2}ds - \frac{2}{\pi}\int_{-a}^{a}\frac{\mu P(s)(x-s)^3}{\left\{(x-s)^2+z^2\right\}^2}ds \tag{16}$$

$$\sigma_z = -\frac{2z^3}{\pi}\int_{-a}^{a}\frac{P(s)}{\left\{(x-s)^2+z^2\right\}^2}ds - \frac{2z^2}{\pi}\int_{-a}^{a}\frac{\mu P(s)(x-s)}{\left\{(x-s)^2+z^2\right\}^2}ds \tag{17}$$

$$\tau_{xz} = -\frac{2z^2}{\pi}\int_{-a}^{a}\frac{P(s)(x-s)}{\left\{(x-s)^2+z^2\right\}^2}ds - \frac{2z}{\pi}\int_{-a}^{a}\frac{\mu P(s)(x-s)^2}{\left\{(x-s)^2+z^2\right\}^2}ds \tag{18}$$

Where σ_x and σ_z describe the stress in the x and z directions while τ_{xz} describes the shear stress in the xz plane. When the two materials in contact have modulus of elasticity an order of magnitude different, the presence of traction may cause a distortion of the pressure profile. However, the pressure profile here is assumed to be unaffected since the friction coefficient, μ, of PTFE sliding against steel is not significant enough to distort the pressure profile from that shown in Figure 5.3.

To analyze the subsurface affects of the asperities, a section of polymer 150 μm long by 200 μm deep was chosen to represent the entire polymer pin. Given the spacing of asperities along the surface, six asperities are in contact with this section of the pin.

The section of polymer was discretized into regions 6 μm long by 10 μm deep. Using the stress equations above, the stress resulting from one of the six asperities was calculated for each of these regions within the main section of polymer. This process was repeated for all six asperities at their respective locations along the surface. The location of the regions remained the same while the distance to the corresponding surface asperity changed. Each asperity's increase in stress on a specific region was summed together to attain the combined stress of all six asperities on that region. Once the total stress of every region was calculated the results were plotted as shown in Figure 5.4, 5.5, and 5.6. Once the original stress and shear state was calculated, the Mohr's circle technique was implemented to find the maximum shear stress within the subsurface. The maximum shear stress at a given depth is given by

$$\sigma_{Avg} = \frac{\sigma_x + \sigma_z}{2} \tag{19}$$

$$R_1 = \left(\sigma_x - \sigma_{Avg}\right)^2 \tag{20}$$

$$R_2 = \left(\tau_{xz}\right)^2 \tag{21}$$

$$\tau_{max} = \sqrt{\left(R_1^2 + R_2^2\right)} \tag{22}$$

Where τ_{max} is the shear stress of the maximum shear stress element. Once τ_{max} is calculated for every location the results were plotted against the Z-axis to reveal the depth at which maximum shear stress occurs. These results can be seen in Figure 5.7.

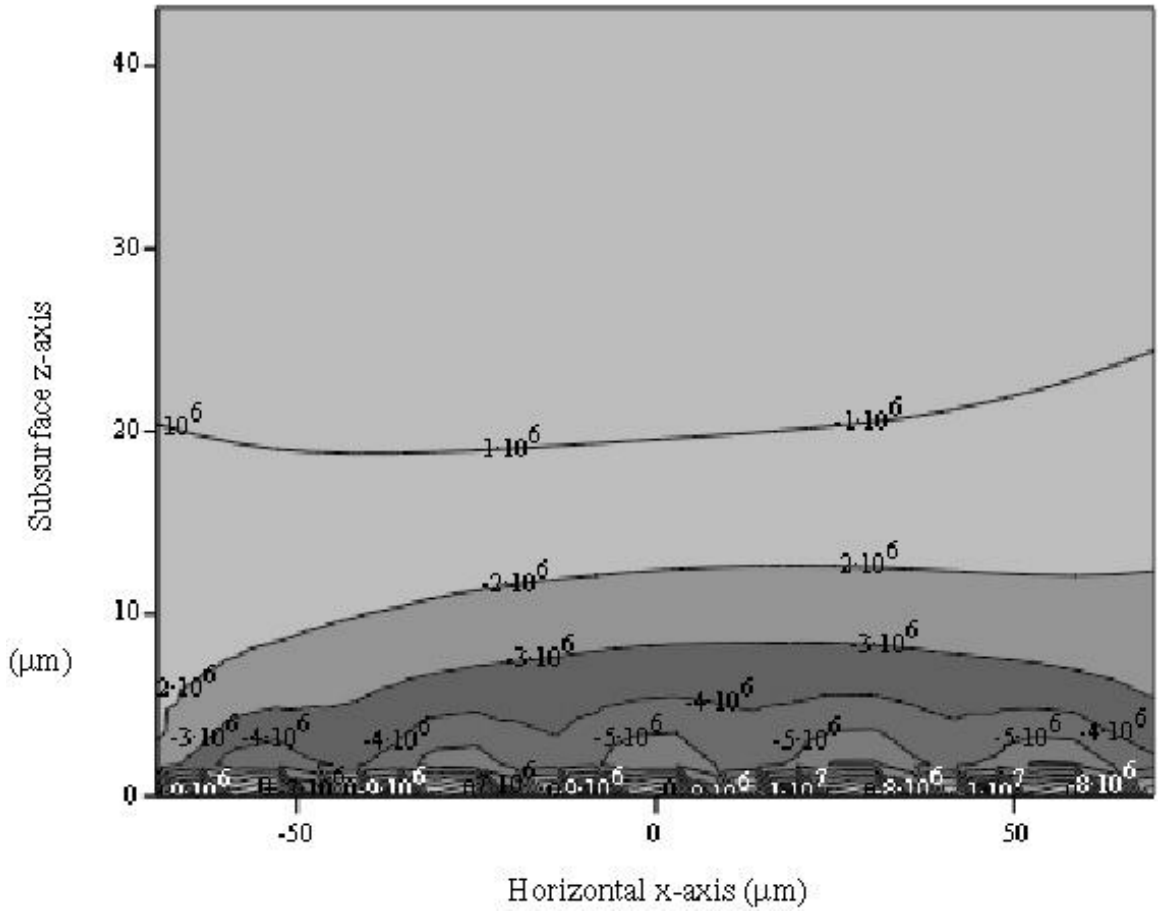

Figure 5.4. Sigma X compressive stress in subsurface of PTFE.

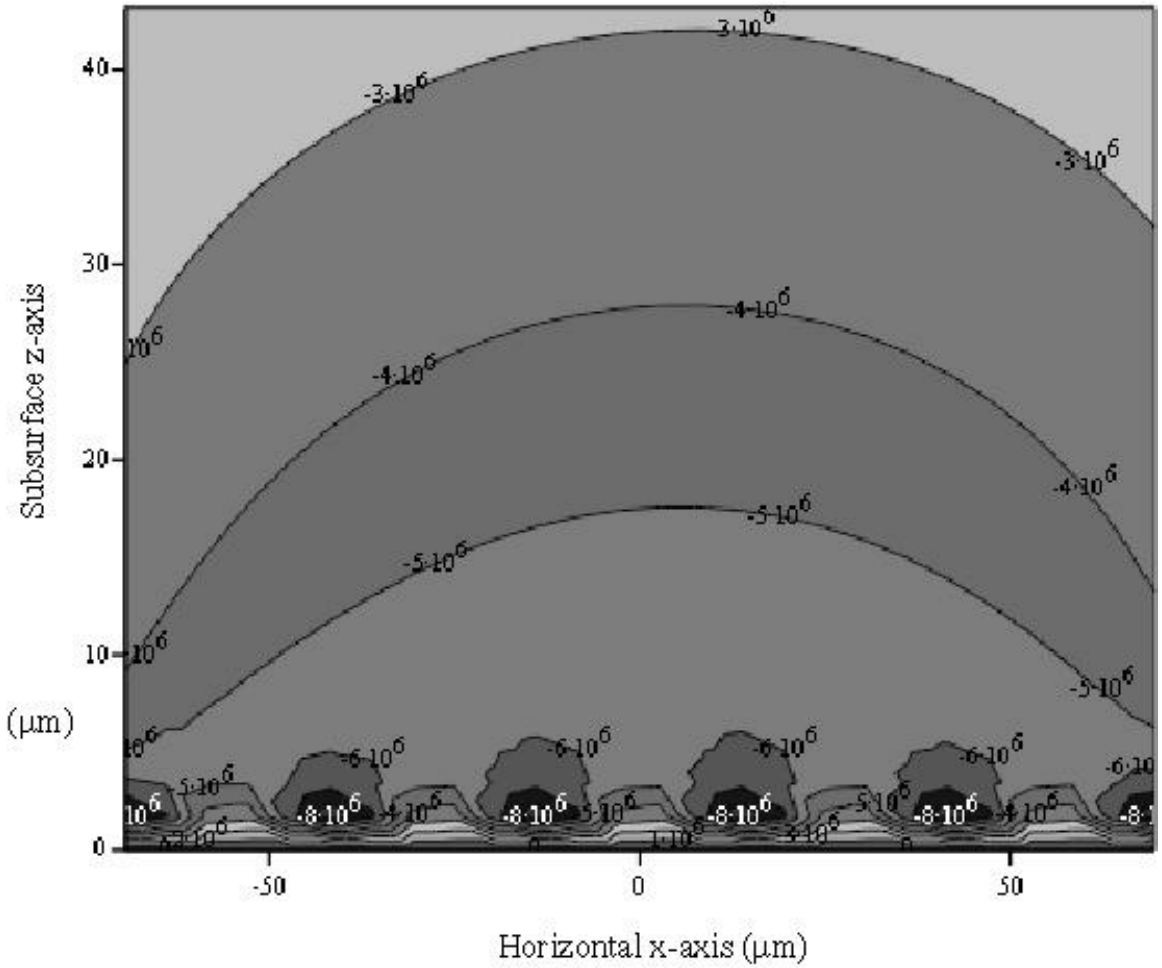

Figure 5.5. Sigma Z compressive stress in subsurface of PTFE.

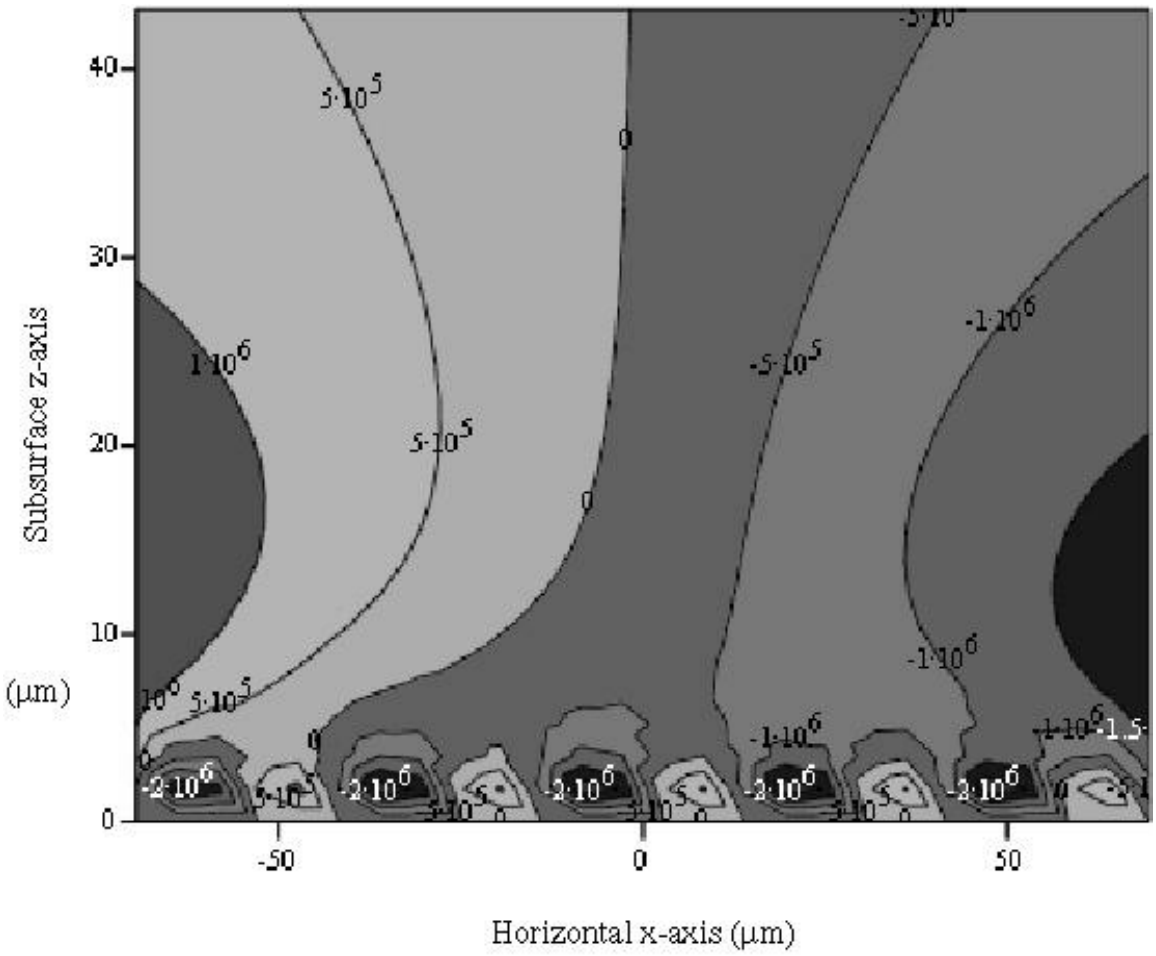

Figure 5.6. Tau XZ shear stress in subsurface of PTFE.

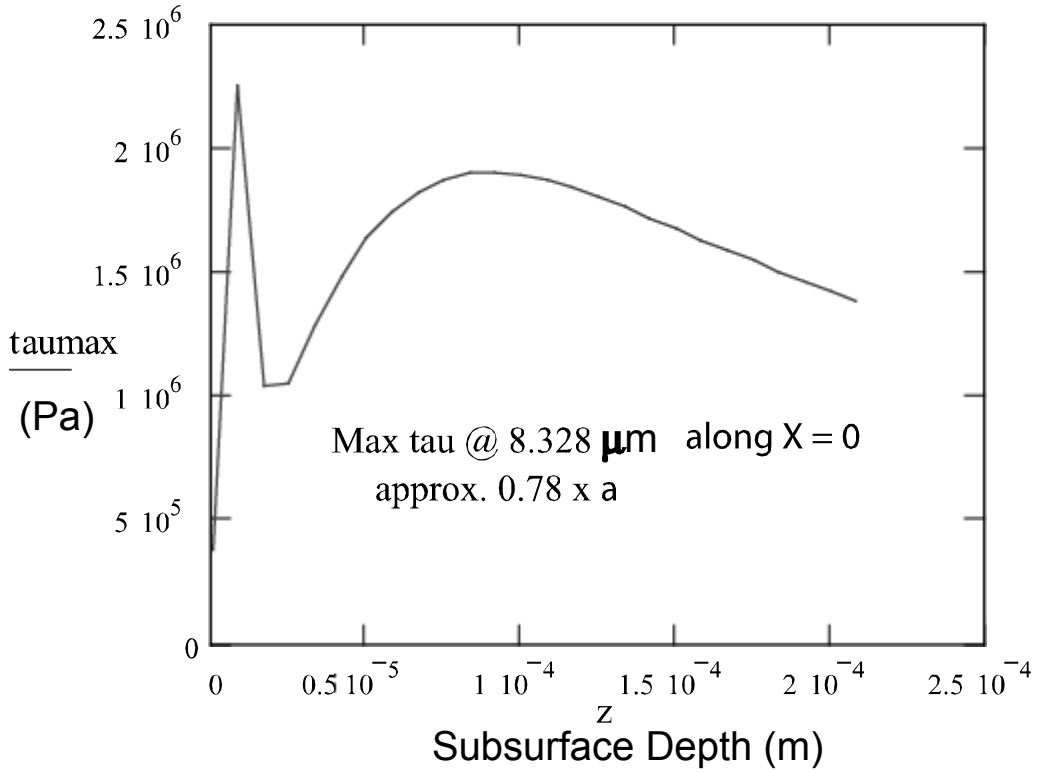

Figure 5.7. Plot of subsurface shear stress along x = 0 indicating shear max.

CHAPTER 6
DISCUSSION

6.1 Delamination

Unlike UHMWPE, PTFE appears to wear at approximately the same rate regardless of any multi-directionality in the sliding motion. Results presented in tests 1-3 and 9 of Table 4A and Figure 4.8 indicate that there is considerable data overlap between wear rates resulting from unidirectional sliding and those resulting from multidirectional sliding. Images from the optical microscopes show that as PTFE wears it tends to form debris as thin plate shaped flakes of material. Wear of UHMWPE is often described as a surface wear process that is dependent on the orientation of the molecular chains relative to the direction of sliding. UHMWPE exhibits low wear under unidirectional sliding because the molecular chains eventually align themselves with the direction of motion, making the chains more difficult to remove from the bulk. The chains are more easily removed when experiencing shear, as is the case under multidirectional sliding. PTFE appears to wear as a result of a subsurface process known as delamination.

Delamination occurs when a subsurface crack propagates long enough to linkup with other subsurface cracks until eventually one crack large enough to break from the bulk is present. The delamination process is depicted in Figures 6.1, 6.2, and 6.3 below. Once sliding begins stresses stemming from the combination of normal load and traction develop within the polymer pin. The stress equations used to model the subsurface stresses experienced by the polymer pin were presented in chapter 5 and have no

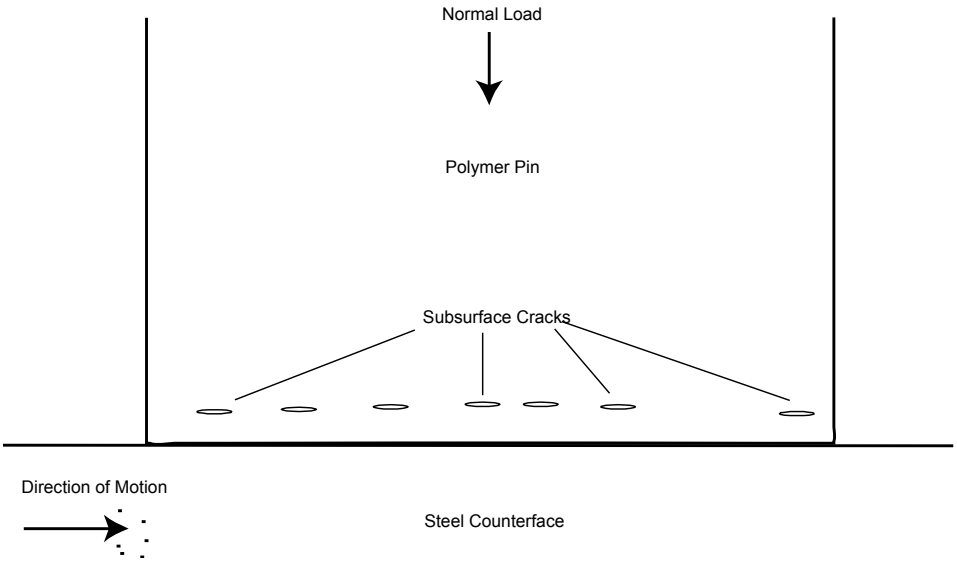

Figure 6.1. Presences of subsurface cracks within polymer pin under stress.

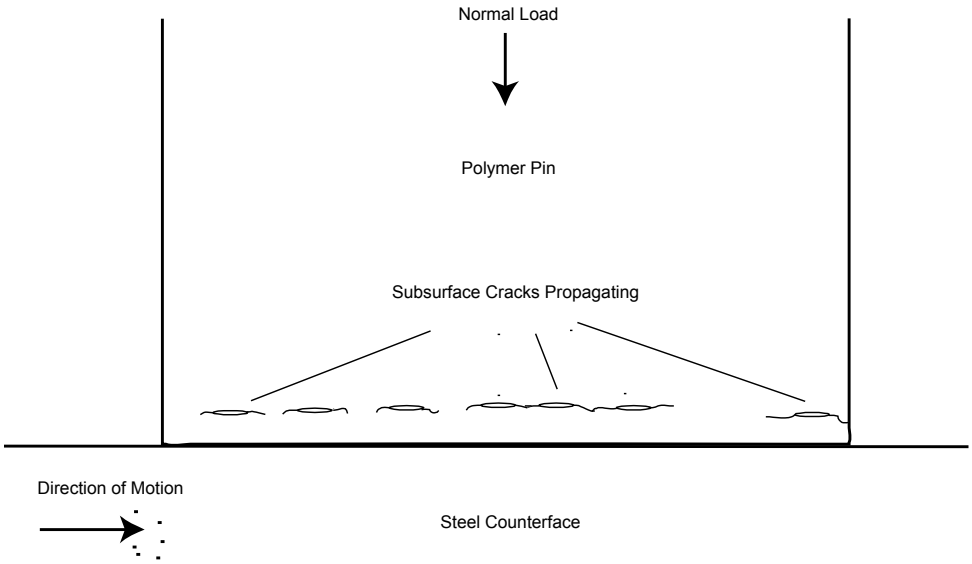

Figure 6.2. Subsurface cracks begin to propagate and link up.

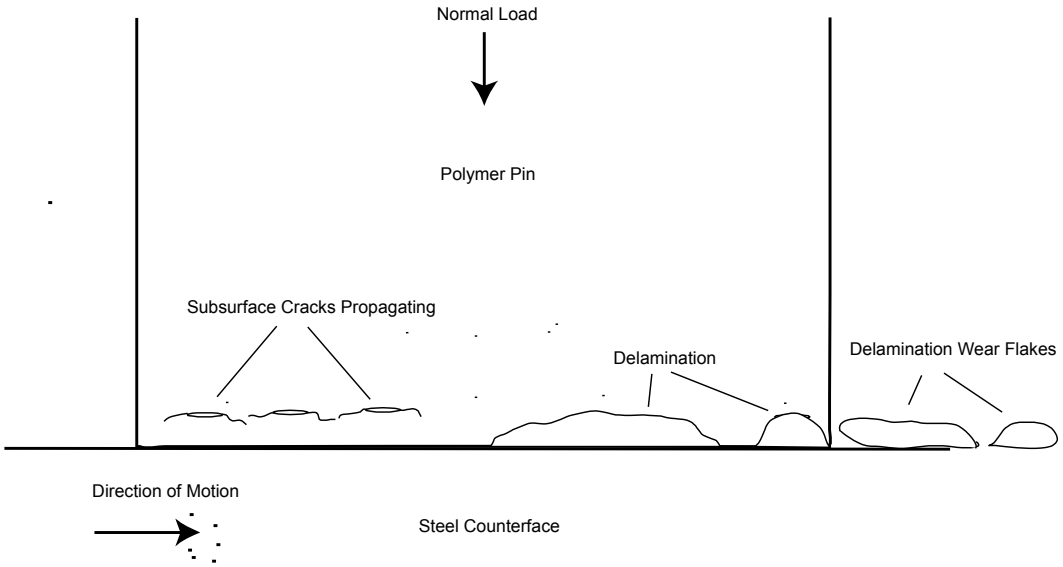

Figure 6.3. Ejections of polymer wear debris resulting from large subsurface crack.

dependence on direction of motion. Therefore, the delamination process has no dependence on direction of sliding. This accounts for the lack of any directional dependence in PTFE sliding wear. Delamination may not influence UHMWPE's wear process because of the extremely low friction values incurred under lubricated sliding.

The pressure profile applied to the polymer surface is the main factor influencing the subsurface stress. The pressure profile depends on both loading and surface topography. For the experiments pertaining to this paper, the only external load applied to the polymer was the normal load. Therefore, modeling the surface topography became the key factor when describing the pressure profile. Depending on the state of stress present in the polymer bulk compression, tension, and shear may be exuded on the imperfections present near the polymer surface. The imperfections include cracks that begin to propagate under either tension or shear. The state of stress depends on the loading and surface features at the polymer/counterface junction. Based on the surface model describing the counterfaces used during wear testing, the stress equations indicate

that both compression and shear are present within the subsurface. Crack propagation may take place by either one or both of the two modes shown in Figure 6.4a, and b.

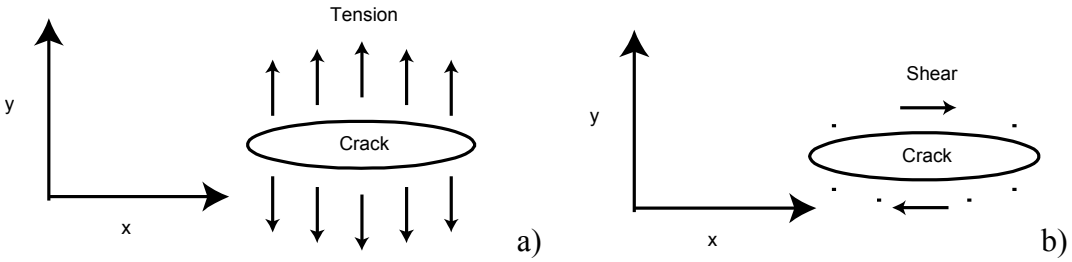

Figure 6.4 Modes of crack propagation a) mode I b) mode II.

Tension, associated with mode I failure, will force the crack to pull apart and thus propagate. Shear will force the top and bottom halves of the crack to move in opposite directions. Mode II is characterized by motion perpendicular to the leading edge of the crack, whereas Mode III the motion is parallel. For the case describing both the counterface and polymer surface topography as sinusoidal with 40 nm amplitude and 30 μm spacing, the subsurface stress model indicates the presence of shear and compression. Given a unidirectional sliding path, mode II propagation best agrees with the subsurface stress model, and indicates that the maximum shear takes place at about 10 μm deep. The correlation between experimental data and theoretical modeling lend support to the theory of delamination as an explanation for the directionally independent wear behavior of PTFE sliding against a polished steel counterface. The subsurface shear present within the subsurface of the polymer results in mode II crack propagation. As the propagation begins to link up several cracks with one another it becomes easier to break a plate of material free from the bulk than to break the polymer/counterface junction. Once a section breaks from the bulk it is either ejected from the wear path as debris or deposited on to the counterface as a transfer film. Although delamination theory accounts for much of what was observed during PTFE wear, it is still unclear as to what mechanism causes

the material to become part of a transfer film instead of ejected as debris. However, it is clear that a full description of PTFE sliding wear behavior must include an explanation for any third body interactions resulting from the transfer film.

6.2 Reversal Zones

An inconsistency between wear tests that employ unidirectional sliding and those that employ multidirectional sliding involves reversal points in the motion path and the subsequent appearance of static friction. A reversal point is any location along the motion path where the polymer pin comes to a stop then restarts its motion in another direction. Such as the endpoints of a linear reciprocating wear path. These locations are of particular interest because they introduce static friction to the sliding process. Motion paths such as circles contain no reversal points since it is not necessary to stop the motion in order to change directions. As can be seen by comparing tests 1-3, 9, and 12 of Table 4A, under identical test conditions, tests that include reversal points have higher wear than tests with no reversal points. Tests 14-16 of Table 4A each include 4 reversal points and possess even higher wear rates than the tests with only 2 reversal points 1-3, and 12. However, the wear path area for tests 14-16 is greater than the area for tests 1-3, and 12. This is significant because an overall view of the data in Table 4A indicates that wear rate increases with increasing wear path area. A comparison could be made between test 13 and tests 14-16. Test 13 has the same wear path area as 14-16, but has only 2 reversal locations. On the average, the wear rate of 14-16 was higher than 13, but some data overlap did occur.

Reversal points are identifiable on the transfer films as interruption areas of broken, patchy film. As stated in the results section of this report, the appearance of broken patchy transfer films was coincident with relatively high wear rates. For smooth

transfer films with reversal points, the same could be said about wear rates over those areas of film interruption. Hence, wear tests have higher wear rates under smooth transfer film formation when reversal points are present in the sliding motion.

6.3 Cycle Dependence in Wear Rate

Figure 4.10 of the results section shows that wear rate has a strong dependence on the number of cycles incurred during sliding. A simple model for this dependence is shown in Figure 6.5.

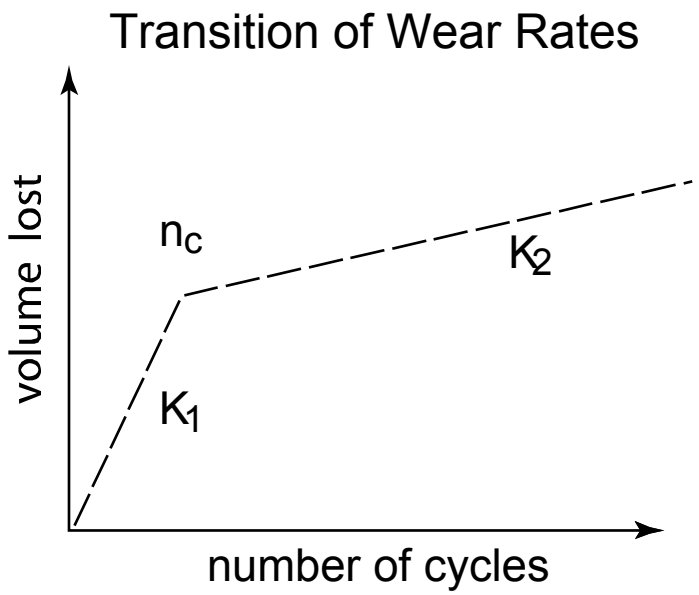

Figure 6.5. Model showing wear rate transition at some critical number of cycles n_c. This model depicts a transition from the initial high wear rate K_1 at some critical number of cycles n_c to a lower steady state wear rate K_2. Therefore, any test that runs beyond n_c will begin to appear more and more like the steady state wear rate. Using linear rules of mixing, a prediction of wear in terms of volume loss for single point measurements can be made using equation 23.

$$V_{loss} = n_c K_1 F_n d + K_2 F_n d(n - n_c) \tag{23}$$

Where d is the total sliding distance divided by the total number of cycles n. An expression based on wear rate of a single point measurement is given by equation 24.

$$K_{sp} = \frac{V_{loss}}{F_n D} = K_2 + \frac{n_c}{n}(K_1 - K_2) \tag{24}$$

Where K_{sp} is the average wear rate over the entire test. Wear at any point during the test can be predicted if the number of cycles at that point is known.

CHAPTER 7
CONCLUSIONS

Changes in wear rate have been observed when changes in test parameters have been implemented. Factors influencing wear rate are load, wear path area, and number of cycles incurred during testing. The influence of number of cycles incurred indicates that wear is driven by the transfer film setup on the counterfaces.

The calculated wear rate values from the pin-on-flat tribometer agreed closely with wear rate values calculated by previous authors. Preliminary testing of this tribometer indicated that the results are repeatable and that changes in wear rate can be attributed to changes in the testing parameters. Therefore, it is believed the tribometer used in this report is functioning properly and can be used to identify factors influencing wear.

1. The initial experiments with cyclic loading suggest that slowly varying cyclic loads have similar wear rates as produced by a constant load equal to the cyclic mean load. This has only been tested for a small range of load that has peak amplitudes that are within the same order of magnitude as the mean load.
2. The qualitative competitive rate models previously proposed for PTFE appear appropriate for explaining the dependence on the number of cycles on wear, but not for the development of the transfer film.
3. The number of reversals in a given wear path is related to wear rate.
4. The directionality of sliding shows significant differences in transfer film morphology within the reversal zones, but does not show significant differences in overall wear rate as compared to linear reciprocating sliding.

There is no satisfactory explanation for how the transfer film develops. Questions concerning transfer film development as well as wear debris growth and expulsion still

remain. A system designed specifically to observe the transfer films development under similar test conditions to those described in this paper is needed to help reveal useful information regarding wear behavior and would serve well as a point of future research. Such a system could be implemented on an existing tribometer with the addition of video imaging equipment and a proper scope setup.

APPENDIX A
MOTION PATH PROGRAMS

```
************************************************************************
constant                ;Program for linear reciprocating motion path
************************************************************************
del constant            ;Clear controller memory of previous program
def constant            ;Define new program

drive10000              ;Activate tables
ma00000                 ;Set table to absolute coordinates
a200,200                ;Set accelerations and decelerations
ad200,200
v9.8425                 ;Set velocities

l                       ;Initiate loop
  d-200000              ;Command table number of units to move
  go1                   ;Initiate table motion
  d200000
  go1
ln                      ;End loop
end                     ;End program



************************************************************************
circle                  ;Program for circular motion path
************************************************************************
del circle              ;Clear controller memory of previous program
def circle              ;Define new program

Drive11000              ;Turn tables on
pv9.8425,9.8425         ;Set path velocities and accelerations and
                        decelerations
pa200
pad200

l1000                   ;Initiate loop
parcop0,0,0,62500       ;Define circle end points (x,y) and center
                        points (x,y)
ln                      ;End loop
                        ;Before this program will run type pcomp circle
                        into the terminal and enter
                        ;Then type prun circle and enter
end                     ;End program
```

```
**********************************************************************
cir                     ;Program for loading and running circular motion
                        path
**********************************************************************
del cir                 ;Clear controller memory of previous program
def cir                 ;Define new program

pcomp circle            ;Compile circle program into controller memory
l200                    ;Initiate loop for 200 cycles
prun circle             ;Run circle program
ln                      ;End loop

end                     ;End program



**********************************************************************
arc2                    ;Program for semi-circular motion path
**********************************************************************
del arc2                ;Clear controller memory of previous program
def arc2                ;Define new program
drive11000              ;Turn tables on

l                       ;Initiate loop
pv9.5                   ;Set path velocities and accelerations
pa1000                  ;Set path accelerations and decelerations
pad1000
prtol5
parcp-127328,0,63664    ;Define arc startpoints (x,y) and end points
                        (x,y)
ln                      ;End loop
                        ;Before this program will run type pcomp arc2
                        into the terminal and enter
                        ;Then type prun arc2 and enter
end                     ;End program



**********************************************************************
constant1               ;Program for 0° diamond motion path
**********************************************************************


del constant1           ;Clear controller memory of previous program
def constant1           ;Define new program

drive11000              ;Activate tables
ma00000                 ;Set tables in absolute/ incremental mode
a200,200                ;Set acceleration to 200 revs/sec^2
ad200,200               ;Set deceleration to 200 revs/sec^2
v7.3159,6.5843,1,1,1

l                       ;Initiate loop
  d-232279,209051       ;Command table number of units to move
  go11                  ;Initiate table motion
  d232279,-209051
  go11
ln                      ;ends loop

end                     ;end main
```

```
*************************************************************************
diamond1                ;Program for 15° diamond motion path
*************************************************************************
del diamond1            ;Clear controller memory of previous program
def diamond1            ;Define new program

drive11000              ;Activate tables
ma00000                 ;Set tables in absolute/ incremental mode
a200,200                ;Set acceleration to 200 revs/sec^2
ad200,200               ;Set deceleration to 200 revs/sec^2

l                       ;Initiate loop
  v5.3625,8.2534        ;Set velocity to 9.8425 revs/sec
  d-44793,68942         ;Command table number of units to move
  go11                  ;Initiate table motion
  v8.7707,4.4665
  d-73263,37309
  go11
  v5.3625,8.2534
  d44793,-68942
  go11
  v8.7707,4.4665
  d73263,-37309
  go11
ln                      ;ends loop

end                     ;end main
```

```
*************************************************************************
diamond2                ;Program for 30° diamond motion path
*************************************************************************
del diamond2            ;Clear controller memory of previous program
def diamond2            ;Define new program

drive11000              ;Activate tables
ma00000                 ;Set tables in absolute/ incremental mode
a200,200                ;Set acceleration to 200 revs/sec^2
ad200,200               ;Set deceleration to 200 revs/sec^2

l                       ;Initiate loop
  v3.0436,9.3601        ;Set velocity to 9.8425 revs/sec
  d-24791,76241         ;Command table number of units to move
  go11                  ;Initiate table motion
  v9.6279,2.0442
  d-78422,16651
  go11
  v3.0436,9.3601
  d24791,-76241
  go11
  v9.6279,2.0442
  d78422,-16651
  go11
ln                      ;ends loop

end                     ;end main
```

```
*************************************************************************
diamond3                ;Program for 45° diamond motion path
*************************************************************************

del diamond3            ;Clear controller memory of previous program
def diamond3            ;Define new program

drive11000              ;Activate tables
ma00000                 ;Set tables in absolute/ incremental mode
a200,200                ;Set acceleration to 200 revs/sec^2
ad200,200               ;Set deceleration to 200 revs/sec^2

l                       ;Initiate loop
  v.51732,9.8289        ;Set velocity to 9.8425 revs/sec
  d4106,78017           ;Command table number of units to move
  go11                  ;Initiate table motion
  v9.8289,.51732
  d78017,4106
  go11
  v.51732,9.8289
  d-4106,-78017
  go11
  v9.8289,.51732
  d-78017,-4106
  go11
ln        ;ends loop

end     ;end main
```

APPENDIX B
RAW DATA

Test	Cylinder	Mass Loss (g)	Normal Load (N)	Sliding Distance (m)	Speed (mm/s)	Path Length (mm)
Linear Recip	1	60	117	670	47	45.7
	2	36	117	670	47	45.7
	3	63	117	670	47	45.7
	4	27	117	670	47	45.7
	5	43	117	670	47	45.7
	6	31	117	670	47	45.7
Linear Recip	1	138	176	670	47	45.7
	2	131	176	670	47	45.7
	3	123	176	670	47	45.7
	4	126	176	670	47	45.7
	5	115	176	670	47	45.7
	6	102	176	670	47	45.7
Linear Recip	1	188	235	670	47	45.7
	2	111	235	670	47	45.7
	3	188	235	670	47	45.7
	4	190	235	670	47	45.7
	5	194	235	670	47	45.7
	6	177	235	670	47	45.7
Linear Recip	1	25	176	670	47	12.7
	4	30	176	670	47	12.7
Linear Recip w/ 0.167 Hz Sinusoidal Load	1	128	147 - 205	670	47	45.7
	2	112	147 - 205	670	47	45.7
	3	149	147 - 205	670	47	45.7
	4	136	147 - 205	670	47	45.7
	5	132	147 - 205	670	47	45.7
	6	123	147 - 205	670	47	45.7
Linear Recip w/ 0.167 Hz Sinusoidal Load	1	98	117 - 235	670	47	45.7
	2	105	117 - 235	670	47	45.7
	3	113	117 - 235	670	47	45.7
	4	112	59 - 293	670	47	45.7
	5	123	59 - 293	670	47	45.7
	6	121	59 - 293	670	47	45.7

Circular 6.35 mm diameter	1	28	117	700	49	19.9
	2	19	117	700	49	19.9
	3	52	176	700	49	19.9
	4	65	176	700	49	19.9
	5	100	235	700	49	19.9
	6	95	235	700	49	19.9
Circular 10.6 mm diameter	1	25	117	700	49	33.2
	2	28	117	700	49	33.2
	3	86	176	700	49	33.2
	4	58	176	700	49	33.2
	5	96	235	700	49	33.2
	6	134	235	700	49	33.2
Circular 15.0 mm diameter	1	45	117	700	49	47.0
	2	42	117	700	49	47.0
	3	105	176	700	49	47.0
	4	82	176	700	49	47.0
	5	147	235	700	49	47.0
	6	134	235	700	49	47.0
Circular 25.4 mm diameter	1	79	117	700	49	79.8
	2	72	117	700	49	79.8
	3	130	176	700	49	79.8
	4	128	176	700	49	79.8
	5	161	235	700	49	79.8
	6	219	235	700	49	79.8
Circular 36.4 mm diameter	1	69	117	700	49	114.3
	2	56	117	700	49	114.3
	3	133	176	700	49	114.3
	4	148	176	700	49	114.3
	5	168	235	700	49	114.3
	6	208	235	700	49	114.3

Spectrum Load	1	162	176 (avg)	670	47	45.7
	2	165	176 (avg)	670	47	45.7
	3	157	176 (avg)	670	47	45.7
	4	178	176 (avg)	670	47	45.7
	5	174	176 (avg)	670	47	45.7
	6	153	176 (avg)	670	47	45.7
Linear Recip	1	145	176	690	48	68.5
	2	148	176	690	48	68.5
	3	162	176	690	48	68.5
	4	145	176	690	48	68.5
	5	152	176	690	48	68.5
	6	159	176	690	48	68.5
Diamond w/ 15^0 Inclusion Angle	1	169	176	620	43	68.5
	2	162	176	620	43	68.5
	3	164	176	620	43	68.5
	4	170	176	620	43	68.5
	5	164	176	620	43	68.5
	6	155	176	620	43	68.5
Diamond w/ 30^0 Inclusion Angle	1	146	176	620	43	68.5
	2	141	176	620	43	68.5
	3	141	176	620	43	68.5
	4	147	176	620	43	68.5
	5	144	176	620	43	68.5
	6	143	176	620	43	68.5
Diamond w/ 45^0 Inclusion Angle	1	110	176	620	43	68.5
	2	105	176	620	43	68.5
	3	105	176	620	43	68.5
	4	113	176	620	43	68.5
	5	104	176	620	43	68.5
	6	102	176	620	43	68.5
Semi-Circular	1	63	117	670	47	45.7
	3	108	176	670	47	45.7
	6	152	235	670	47	45.7

APPENDIX C
SHOP DRAWINGS

Shop drawing of aluminum base mounted to tribometer stage.

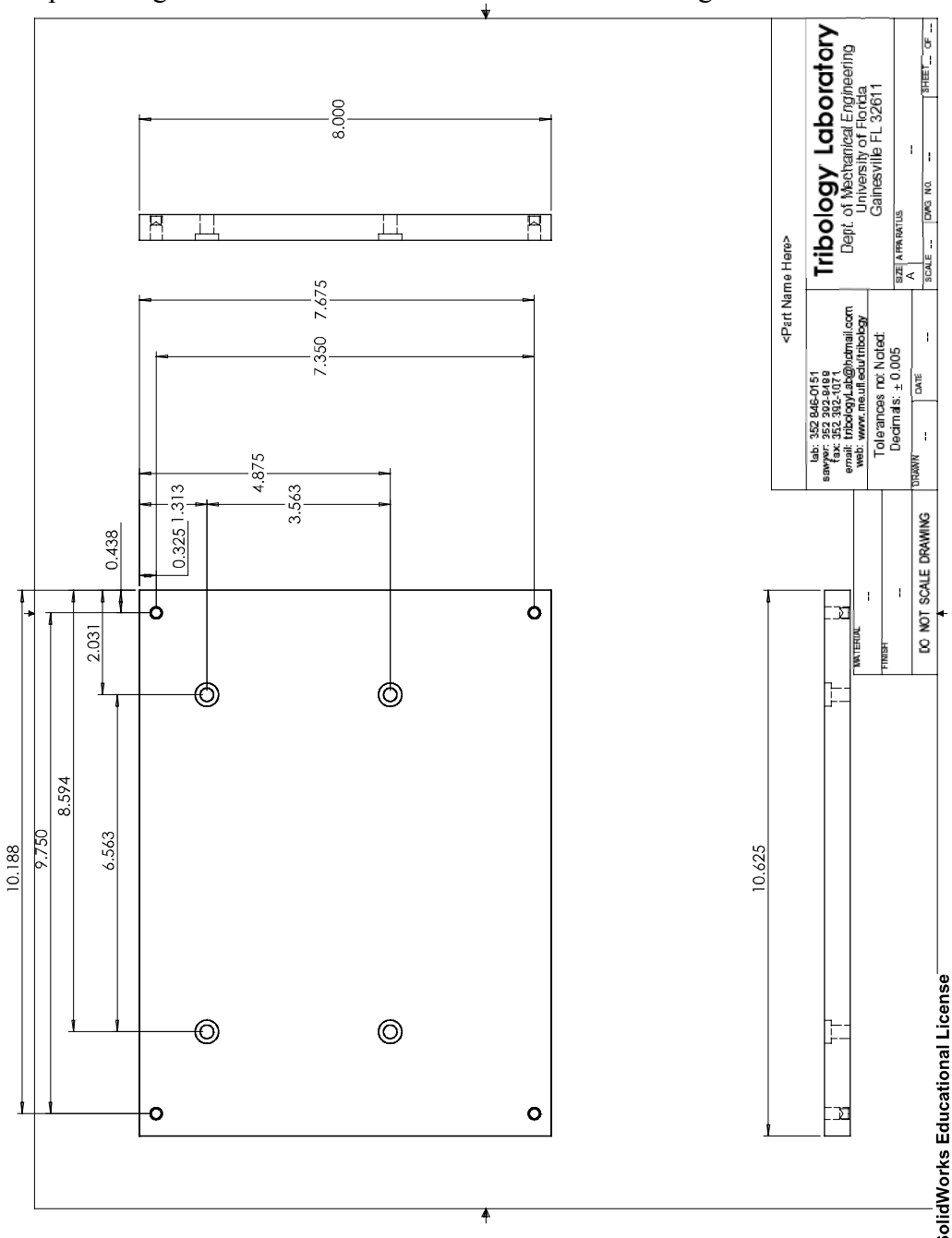

Shop drawing of counterface mount.

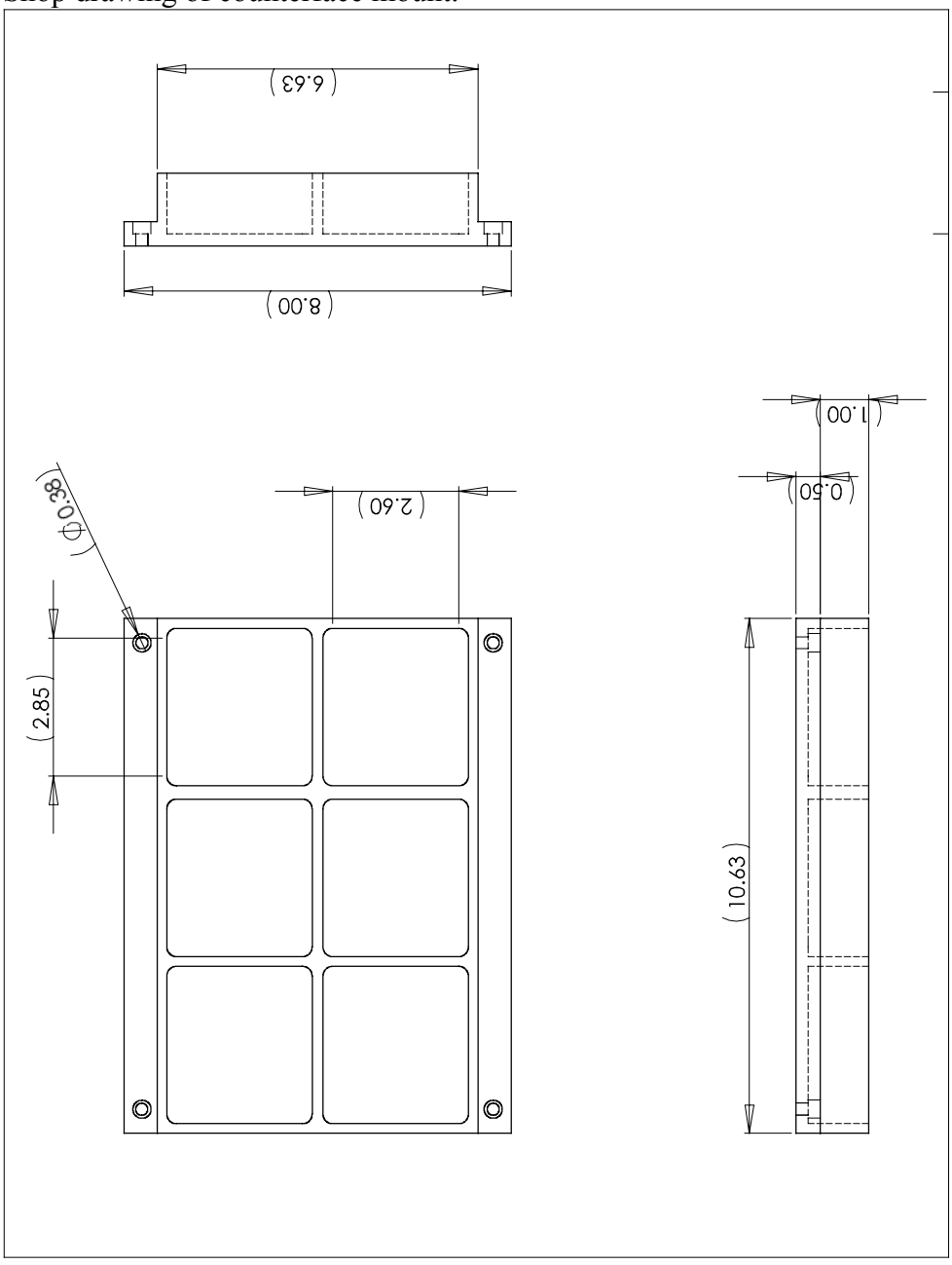

Shop drawing of polymer pin sample.

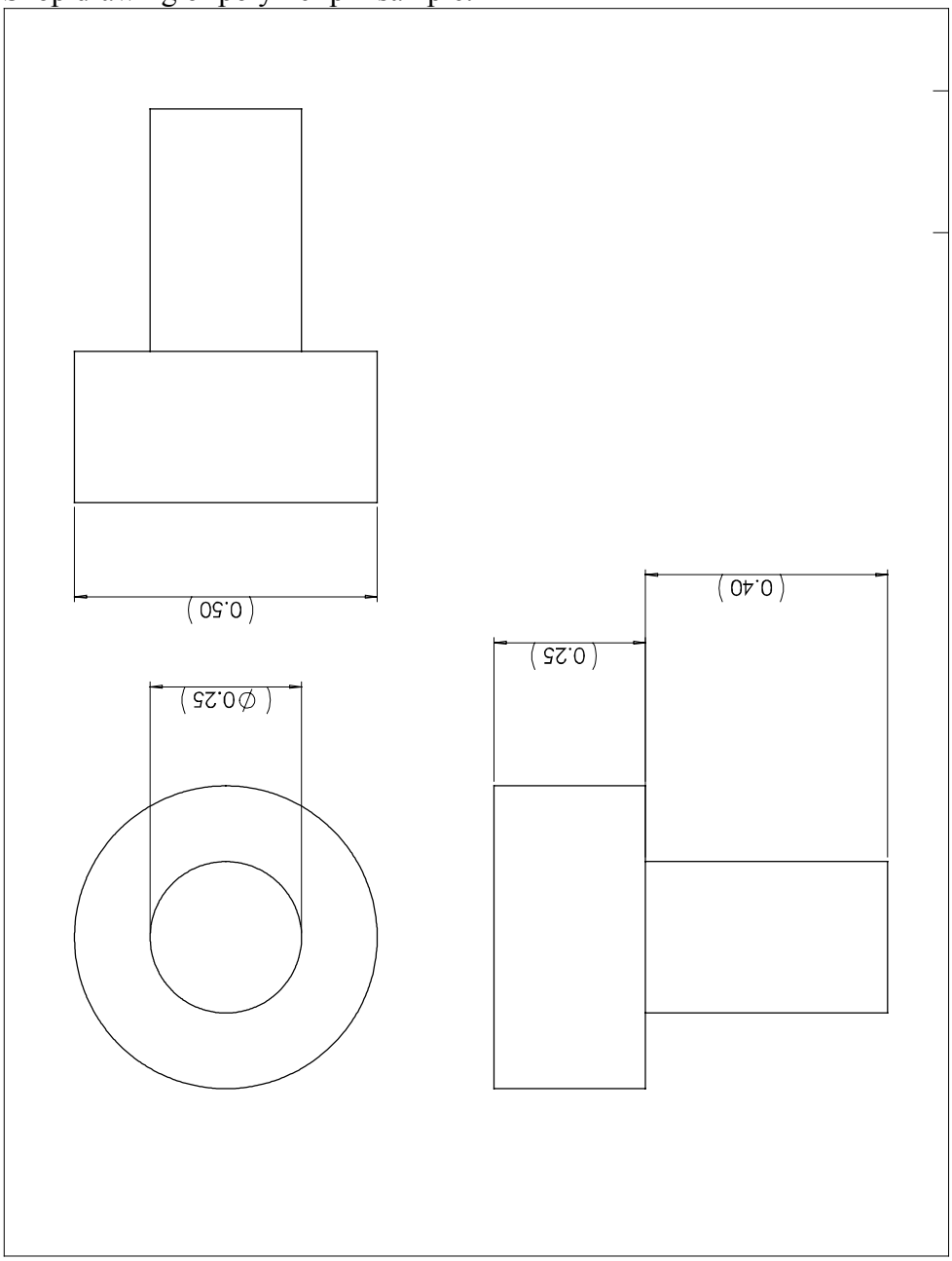

Shop drawing of polymer sample holder.

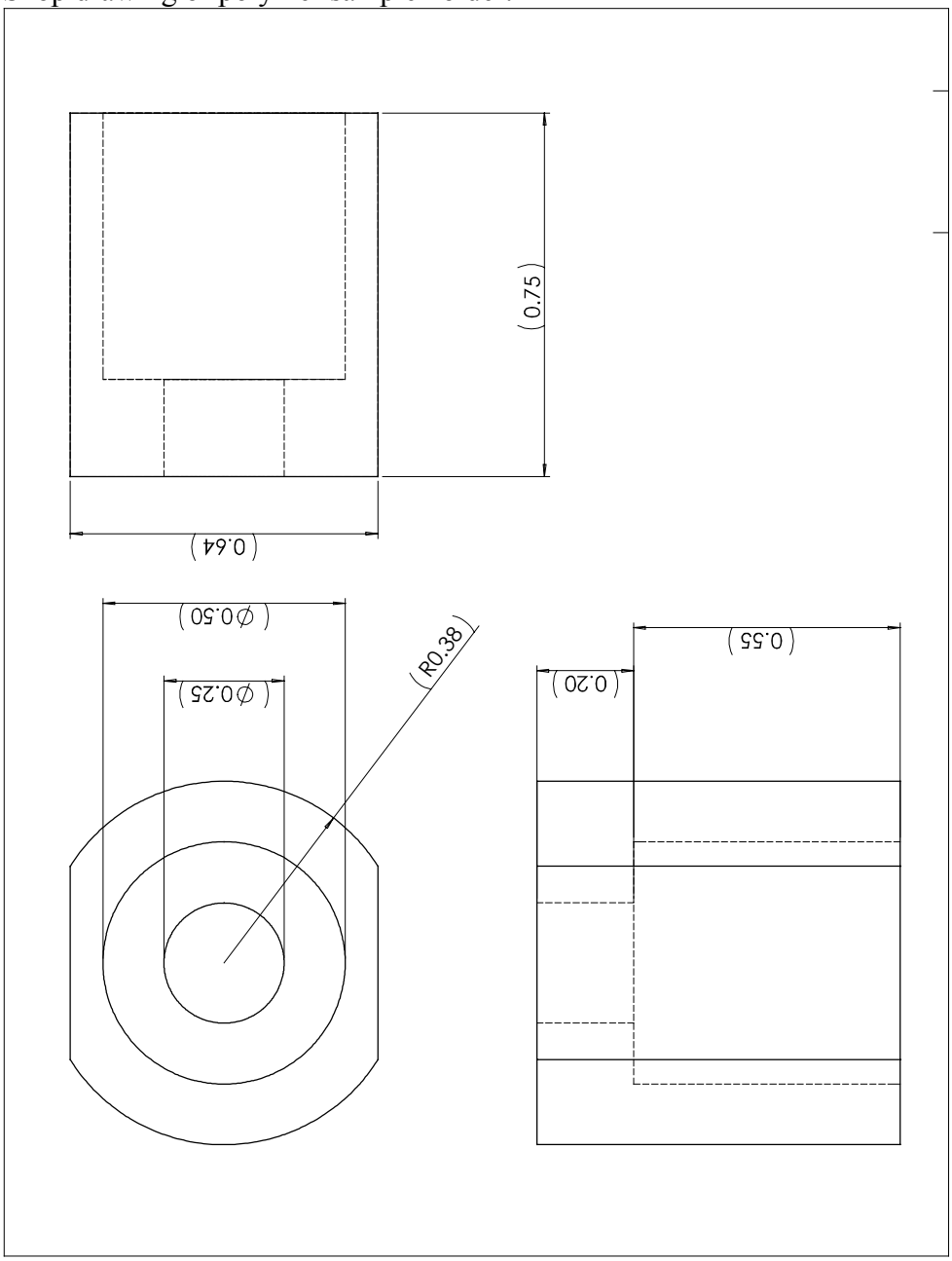

APPENDIX D
SURFACE METROLOGY

Surface profiles of steel counterfaces.

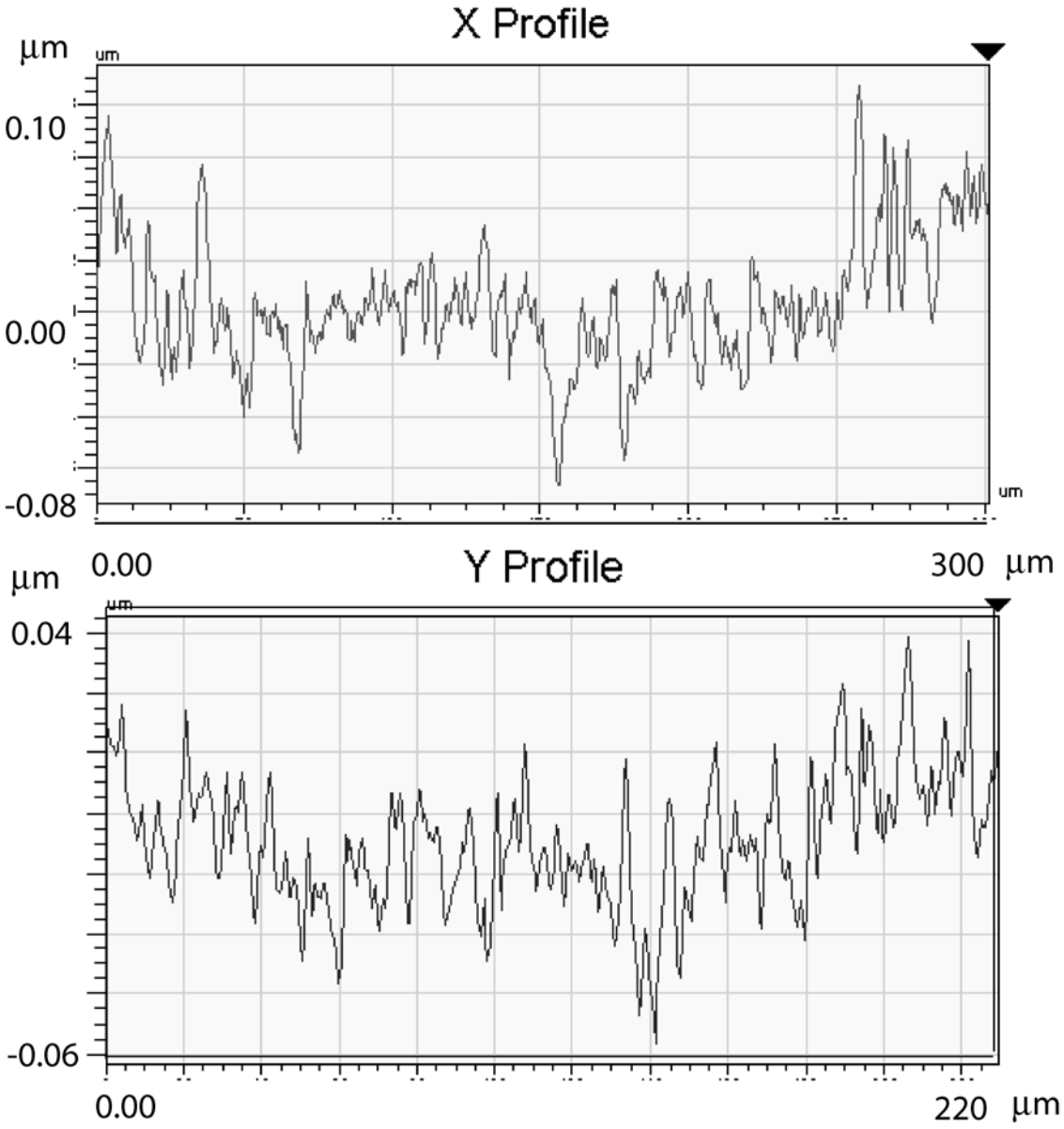

LIST OF REFERENCES

1. Tanaka K., Uchiyama Y., and Toyooka S., The Mechanism of Wear of Polytetrafluoroethylene, Wear 23, pp 153-172 (1973)

2. Tanaka K.,and Miyata T., Studies on the Friction and Transfer of Semi-Crystalline Polymers, Wear 41, pp 383-398 (1977)

3. Schott M., Preparation and Properties of Highly Oriented Polytetrafluoroethylene Films, Synthetic Metals 67, pp 55-61 (1994)

4. Bodo P., and Schott M., Highly Oriented Polytetrafluoroethylene Films: A Force Microscopy Study, Thin Solid Films 286, pp 98-106 (1996)

5. Viswanath N., and Bellow D. G., Development of an Equation for the Wear of Polymers, Wear 181-183, pp 42-49 (1995)

6. Yang E-L., Hirvonen J. P., and Toivanen R. O., Effect of Temperature on the Transfer Film formation in sliding Contact of PTFE With Stainless Steel, Wear 146, pp 367-376 (1991)

7. Blanchet T. A., and Peng Y-L., Wear-Resistant Polytetrafluoroethylene via Electron Irradiation, Lubr. Eng. 52, pp 489-495 (1995)

8. Briscoe B., Wear of Polymers: An Essay on Fundamental Aspects, Tribol. Int. 14, pp 231-243 (1981)

9. Briscoe B. J., and Stolarski T. A., Transfer Wear of Polymers During Combined Linear Motion and Load Axis Spin, Wear 104, pp 121-137 (1985)

10. Vijayan K., and Biswas S. K., Wear of Polytetrafluoroethylene: Some Crystallographic Observations, Wear 150, pp 267-273 (1991)

11. Brainard W. A., and Buckley D. H., Adhesion and Friction of PTFE in Contact With Metals as Studied by Auger Spectroscopy, Field Ion and Scanning Electron Microscopy, Wear 26, pp 75-93 (1973)

12. Cheng X., Xue Y., and Xie C., Tribological Investigation of PTFE Composite Filled With Lead and Rare Earths-Modified Glass Fiber, Materials Letters 4198, pp 1-5 (2002)

13. Wieleba W., The Statistical Correlation of the Coefficient of Friction and Wear Rate of PTFE Composites With Steel Counterface Roughness and Hardness, Wear 252, pp 719-729 (2002)

14. Jintang G., Tribochemical Effects in Formation of Polymer Transfer Film, Wear 245, pp 100-106 (2000)

15. Pleskachevsky Y. M., and Smurugov V. A., Thermal Fluctuations at PTFE Friction and Transfer, Wear 209, pp 123-127 (1997)

16. Blanchet T. A., and Peng Y-L., Wear Resistant Irradiated FEP/Unirradiated PTFE composites, Wear 214, pp 186-191 (1998)

17. Sui H., Pohl H., Schomburg U., Upper G., and Heine S., Wear and Friction of PTFE Seals, Wear 224, pp 175-182 (1999)

18. Briscoe B. J., Evans P. D., Pelillo E., and Sinha S. K., Scratching Maps for Polymers, Wear 200, pp 137-147 (1996)

19. Wang A., A Unified Theory of Wear for Ultra-High Molecular Weight Polyethylene in Multi-Directional Sliding, Wear 248 (2001), pp 38-47 (2001)

20. Muratoglu O. K., Bragdon C. R., O'Connor D. O., Jasty M., H. Harris W. H., Gul R., and McGarry F., Unified Wear Model for Highly Crosslinked Ultra-High Molecular Weight Polyethylenes, Biomaterials 20, pp 1463-1470 (1999)

21. Schmalzried T. P., and Callaghan J. J., Current Concepts Review Wear in Total Hip and Knee Replacements, The Journal of Bone and Joint Surgery, Incorporated 81-A, pp 115-136 (1999)

22. Burroughs B. R.,and Blanchet T. A., Factors Affecting the Wear of Irradiated UHMWPE, Society of Tribology and Lubrication Engineers Presentation NY (2000)

23. Suh N. P., The Delamination Theory of Wear, Wear 25, pp 111-124 (1973)

24. Steijn R. P., The Sliding Surface of Polytetrafluoroethlene: An Investigation with the Electron Microscope, Wear 12, pp 193-212 (1968).

25. Gong D., Xue Q., and Wang H., Physical Models of Adhesive Wear of Polytetrafluoroethylene and its Composites, Wear 147, pp 9-24 (1991)

26. Collins J. A., Failure of Materials in Mechanical Design, 2nd Edition, A Wiley-Interscience Publication NY, NY (1993)

27. Johnson K. L., Contact Mechanics, Cambridge University Press Cambridge, UK (1985)

BIOGRAPHICAL SKETCH

Darren McGuire was born the second son of Joseph and Louise McGuire September 2nd, 1976. Darren lived in Wappingger Falls, New York until the age of 11 when he and his parents moved to beautiful Flagler Beach, Florida. Darren began his engineering career at Santa Fe Community College and then transferred to the University of Florida where he received his Bachelor of Science degree. After receiving the University of Florida alumni fellowship award he went on to pursue his Master of Science in the field of tribiology.